THE JOURNAL OF PHYSICAL CHEMISTRY B

Article

Cite This: J. Phys. Chem. B 2018, 122, 3572−3586

pubs.acs.org/JPCB

Response of Membranes and Vesicles to Capillary Forces Arising from Aqueous Two-Phase Systems and Water-in-Water Droplets

Reinhard Lipowsky*

Theory & Biosystems, Max Planck Institute of Colloids and Interfaces, 14424 Potsdam, Germany

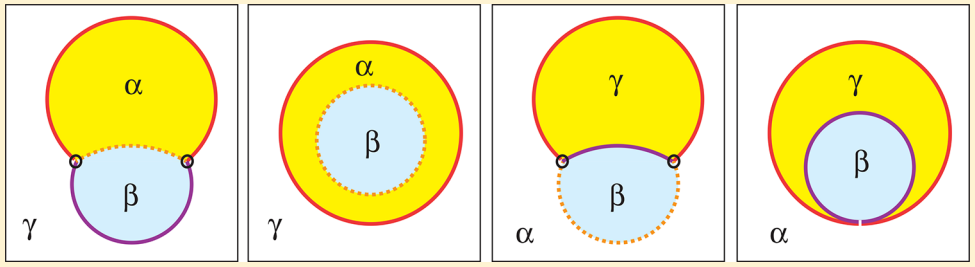

ABSTRACT: Aqueous two-phase systems and water-in-water emulsions have attracted much recent interest. Here, we theoretically study the interactions of such systems with biomimetic membranes and giant unilamellar vesicles (GUVs). For partial wetting, the water−water interface and the membrane form a three-phase contact line that partitions the membrane into two distinct segments with different tensions and different curvature-elastic properties. On the nanometer scale, the capillary forces arising from the water−water interface lead to a smoothly curved membrane that forms an intrinsic contact angle with the interface. The corresponding balance conditions are derived here for general curvature-elastic parameters of the two membrane segments. On the micrometer scale, the capillary forces deform the membrane segments into spherical caps with an apparent kink along the contact line. A new computational method is introduced by which these piece-wise spherical vesicle shapes can be analyzed in a systematic manner. The method is based on a general relationship that is reminiscent of Neumann's triangle but depends explicitly on the curvatures of the membrane segments. For certain regions of the parameter space, corresponding to small or large spontaneous curvatures, the force balance along the apparent contact line can be described in a self-consistent manner and then leads to curvature-independent relationships that involve the total membrane tensions. The different relationships can be used to determine the material parameters of the droplet−vesicle system from the observed morphologies of the GUVs. The approach described here is quite general and can be applied to different membrane compositions and aqueous two-phase systems. The same computational approach can also be used to elucidate the response of biological membranes to the recently discovered membrane-less, droplet-like organelles.

INTRODUCTION

Aqueous two-phase systems, also called aqueous biphasic systems, have been used for a long time in biochemical analysis and biotechnology and are intimately related to water-in-water emulsions.[1,2] Renewed interest in these systems arose from several recent developments such as the use of ionic liquids,[3] improved control of the biphasic partitioning of biomolecules,[4,5] the production and handling in microfluidic devices,[6] and the Pickering stabilization of water-in-water droplets by various types of particles.[7−10] Aqueous two-phase systems based on biopolymers such as PEG and dextran undergo phase separation when the weight fractions of the polymers exceed a few percent. The corresponding interfacial tensions are ultralow, of the order of 10^{-7}−10^{-4} N/m, reflecting the vicinity of a critical demixing point in the phase diagram.[11−14]

When two liquid phases partially wet an extended surface, the liquid−liquid interface forms a contact line and certain contact angles with this surface. For a solid or rigid surface, the associated contact angle is governed by Young's equation arising from the balance of the force components tangential to the surface. When the surface represents another liquid−liquid interface with a third liquid phase, the force balance along the contact line leads to Neumann's triangle that describes this balance both in the tangential and in the normal direction.[15] These force balance equations are quite general and apply to any phase-separated liquid including aqueous two-phase systems. For two aqueous phases in contact with rigid surfaces, the contact angles have been recently measured for a variety of surface materials in the context of Pickering stabilization.[7−10]

In this paper, we consider aqueous two-phase systems in contact with biomimetic membranes such as lipid bilayers, which represent surfaces with unusual properties. First, similar to liquid−liquid interfaces, these membranes are two-dimensional fluids and characterized by fast lateral diffusion. As a consequence, they can change their local composition in response to the molecular interactions with their local aqueous environment. Therefore, when a multicomponent membrane is in contact with two

Special Issue: Benjamin Widom Festschrift

Received: October 31, 2017
Revised: January 30, 2018
Published: February 21, 2018

DOI: 10.1021/acs.jpcb.7b10783
J. Phys. Chem. B 2018, 122, 3572−3586

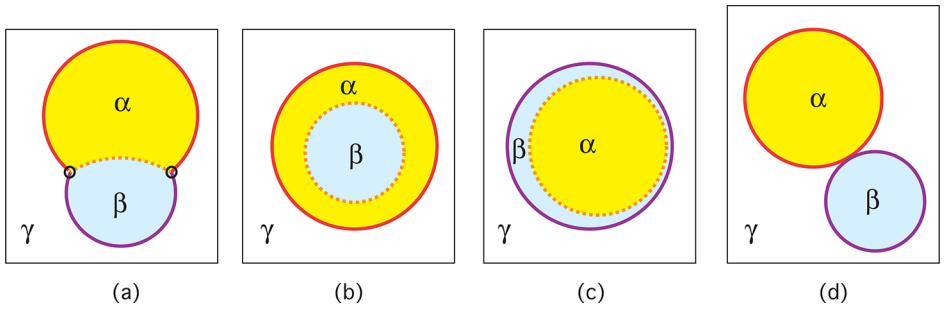

Figure 1. In-wetting morphologies arising from phase separation into two aqueous phases, α (yellow) and β (blue), *within* a giant vesicle. The vesicle is surrounded by the bulk liquid γ (white) which plays the role of an inert spectator phase. Red and purple segments of the vesicle membrane are in contact with the α and β droplets, respectively. The $\alpha\beta$ interfaces are depicted as dashed orange lines: (a) Partial wetting of the vesicle membrane by both the α and the β phase. This morphology exhibits a three-phase contact line (black circles). On the micrometer scale, the vesicle shape exhibits a kink along this contact line which directly reveals the capillary forces acting onto the vesicle membrane. (b) Complete wetting of the membrane by the α phase. (c) Complete wetting by the β phase. (d) Special morphology for which the α and the β droplet are separated by a closed membrane neck. The latter morphology, which resembles complete wetting by the γ phase, is only possible if the membrane has a certain minimal area to enclose both spherical droplets completely.

aqueous phases, α and β, it is partitioned into two types of segments that will, in general, differ in their molecular composition. Second, in contrast to liquid−liquid interfaces, the shape of membranes is usually dominated by curvature elasticity.[16−19] The latter type of elasticity involves two material parameters, bending rigidity and spontaneous (or preferred) curvature, both of which depend on the molecular composition of the membranes and on their molecular interactions with the aqueous environment. As a consequence, the membrane segments in contact with the α and β phases will in general have different curvature-elastic properties. Third, the membranes are so flexible that they can undergo strong morphological changes in response to the capillary forces arising from the water−water interfaces even though these interfaces are characterized by ultralow interfacial tensions.

Contact angles between water−water interfaces and membranes were first measured for giant unilamellar vesicles (GUVs) formed by lipid bilayers in contact with PEG−dextran solutions.[20] In the latter case, it is possible to confine the aqueous phase separation to the interior compartments of the GUVs. For the PEG−dextran systems, two methods have been used to achieve such a confinement. First, the system was prepared at a sufficiently high temperature at which the polymer solution forms a uniform liquid and phase separation was then initiated by cooling the system down.[21−23] Second, the system was prepared at room temperatue and the GUVs were then osmotically deflated by increasing the osmolarity of the exterior solution.[20,24−26] The permeation of water from the interior to the exterior solution increases the weight fractions of the polymers within the interior solution which then undergoes phase separation. Temperature changes affect both the vesicle volume and the membrane area, whereas osmotic deflation changes only the vesicle volume and keeps the membrane area unchanged.

Phase separation into two aqueous phases, α and β, within a GUV can lead to different in-wetting morphologies, as displayed in Figure 1. For all morphologies, the vesicle is surrounded by a third aqueous phase γ that plays the role of an inert spectator phase. The morphologies in Figure 1a and b have been observed by optical microscopy for phase separated PEG−dextran solutions which eventually form one PEG-rich α and one dextran-rich β droplet inside the GUV.[20,24−26] The morphology in Figure 1a corresponds to partial wetting of the vesicle membrane by both α and β, and the morphology in Figure 1b, to complete wetting by the PEG-rich α phase. The partial wetting morphology is characterized by a three-phase contact line at which the $\alpha\beta$ interface between the two liquid phases meets the vesicle membrane and partitions the membrane into two segments. The partially wetted shapes were observed to have an apparent kink close to this contact line,[24,25] as schematically shown in Figure 1a. In addition, the shapes of the partially wetted membranes form piece-wise spherical caps, quite different from the smoothly curved shapes that the membranes form in the absence of partial wetting and capillary forces. The same three-spherical-cap morphology applies to two liquid droplets composed of the phases α and β that coexist with the bulk liquid γ in the absence of the vesicle, as will be discussed further below.

Wetting of vesicle membranes has also been observed when the PEG−dextran solutions underwent phase separation outside the GUVs.[27] In the latter case, the aqueous minority phase forms aqueous droplets that can interact with the vesicle membrane, leading to different out-wetting morphologies. The main body of this paper will focus on the case of in-wetting; the behavior of out-wetting will be briefly discussed at the end.

The apparent kink in the membrane shape as observed for partial wetting, see Figure 1a, directly reveals the capillary forces that the $\alpha\beta$ interface exerts onto the vesicle membrane. These forces are balanced by tensions in the two membrane segments. One objective of the present paper is to elucidate this force balance between the $\alpha\beta$ interface and the vesicle membrane along the contact line. Previous theoretical studies of this balance have been quite limited. The first study was based on energy minimization of axisymmetric vesicle−droplet shapes under the assumption that both membrane segments have the same curvature-elastic properties and zero spontaneous curvatures.[24] Later experiments revealed, however, that one of the two membrane segments formed many nanotubes which implies a large spontaneous curvature of this segment.[25,28] In order to address these observations, a second theoretical approach was based on the assumption that the balance between the interfacial tension of the water−water interface and the tensions in the two membrane segments can be described by a generalized Neumann's triangle. The latter approach is appealing from an intuitive point of view but remains to be justified, in particular because the membrane tensions are composite in nature and consist of several contributions that are generated by different mechanisms.

Here, we will first reconsider axisymmetric vesicle−droplet shapes and derive the balance between capillary forces and

DOI: 10.1021/acs.jpcb.7b10783
J. Phys. Chem. B 2018, 122, 3572−3586

membrane tensions without any simplifying assumptions about the curvature-elastic properties of the two membrane segments. The resulting equation contains additional terms that depend on the highly curved membrane shape along the contact line. At present, this balance equation cannot be used to analyze the GUV shapes obtained by optical microscopy because the microscopy images do not resolve the highly curved membrane shape along the contact line but exhibit an apparent kink instead. On the other hand, the experimental observations revealed one universal feature of the partial wetting morphologies, namely, that the shapes of the two membrane segments are very well described by spherical caps that meet at an apparent contact line; see Figure 1. As shown below, the spherical caps are described by shape equations that depend on the curvature radii of the spherical segments and on certain combinations of curvature-elastic parameters. Because the curvature radii can be directly obtained by optical microscopy, these shape equations can be used to deduce the curvature-elastic properties of both membrane segments. In addition, starting from the (free) energy of the spherical cap segments, force balance equations along the apparent contact line can also be obtained which are shown to apply to certain regimes of the curvature-elastic parameters.

In the experimental studies of deflation-induced phase separation and in-wetting by PEG−dextran solutions,[25,26] the adsorption of PEG molecules onto the membrane generated a relatively large spontaneous curvature of the membrane segments that were in contact with the PEG-rich liquid phase. In order to relax the spontaneous tension of the weakly curved GUV membranes,[28] these membranes formed membrane nanotubes that protruded into the vesicle interior. For partial wetting, the nanotubes accumulated at the liquid−liquid interface between the PEG-rich and the dextran-rich droplet in order to form additional three-phase contact lines along the tubes. Thus, deflation of the PEG−dextran solutions led simultaneously to both wetting and tubulation of the GUVs. However, these two processes do not have to be coupled and can occur independently. First, nanotubes can be formed in the absence of aqueous phase separation, as observed experimentally for GUVs exposed to asymmetric PEG solutions without dextran.[26] Second, membrane wetting is expected to always generate some spontaneous curvature but tubulation can only occur if the spontaneous curvature is sufficiently large compared to the inverse vesicle size. In the following, we will focus on wetting and first ignore the possibility of tube formation. The additional aspects related to spontaneous tubulation will be addressed further below.

The paper is organized as follows. The next section on "Theoretical Description" describes the different energy terms of the vesicle−droplet systems and clarifies the composite nature of membrane tension by considering the adhesion free energies between the membrane and the aqueous phases and by including an additional term corresponding to the lateral membrane stress that acts to stretch (or compress) the membrane. Both the adhesion terms and the lateral stress term contribute to the general shape functional for the vesicle shape and to the corresponding Euler−Lagrange or shape equations for the two membrane segments as obtained from the first variation of the shape functional. The shape equations simplify for spherical membrane segments and are then applied to the partial wetting morphology in Figure 1a. We also examine the (free) energy of the spherical cap segments and derive tension−angle relationships that apply to certain regions of the parameter space and describe the force balance along the apparent contact line. Another in-wetting morphology that will be discussed is the special morphology in Figure 1d which involves a closed membrane neck. The paper concludes with a brief discussion of out-wetting morphologies and some perspectives for future work on wetting of membranes and vesicles.

THEORETICAL DESCRIPTION

Basic Assumptions about the Composition of the Vesicle Membrane. As mentioned before, multicomponent membranes exposed to two different aqueous solutions are partitioned into two segments that will, in general, differ in their molecular compositions, as illustrated in Figure 1a. These different compositions reflect the different molecular interactions between the membrane molecules and the two aqueous phases. Membrane segmentation can also arise via two alternative mechanisms. One such mechanism is provided by phase separation within the membranes which leads to two types of membrane phases that differ in their lipid or lipid−protein composition. Another alternative mechanism for segmentation corresponds to curvature sorting, i.e., the preference of some membrane molecules for highly curved membrane segments.

Here, we consider membrane compositions that belong to the one-phase region when the vesicle membrane is exposed to a uniform aqueous environment provided by any of the three liquid phases α, β, and γ. Furthermore, we will assume that curvature sorting of the membrane components is negligible and can be ignored. In such a situation, the different molecular compositions of the $\alpha\gamma$ and $\beta\gamma$ membrane segments are determined by the different molecular interactions of the membrane molecules with the two distinct aqueous phases, molecular interactions that will be described by the corresponding adhesion free energies.

Geometry of Partial Wetting Morphology. The partial in-wetting morphology in Figure 1a involves two droplets of α and β phase with volumes V_α and V_β. The total volume of the vesicle is then given by $V = V_\alpha + V_\beta$. The two droplet volumes are bounded by three surface segments: the $\alpha\beta$ interface between the α and the β droplet as well as two membrane segments, the $\alpha\gamma$ segment in contact with the α droplet and the $\beta\gamma$ segment exposed to the β droplet. All three surface segments meet along the three-phase contact line.

The $\alpha\beta$ interface has the area $A_{\alpha\beta}$ that can change in order to adapt to changes in the droplet volumes and in the vesicle shape. The two membrane segments have the areas $A_{\alpha\gamma}$ and $A_{\beta\gamma}$ which add up to the total area $A = A_{\alpha\gamma} + A_{\beta\gamma}$ of the vesicle membrane. Because of the ultralow solubility of the lipid molecules and the low area compressibility of the membrane, the value of the total membrane area A is essentially fixed at constant temperature. More precisely, the area dilation, $(A - A_0)/A_0$, from a relaxed membrane state with area A_0 is related to the lateral membrane stress Σ via the area compressibility modulus K_A according to $\Sigma = K_A \frac{A - A_0}{A_0}$. For the wetting morphologies considered here, the lateral stresses that act on the GUV membranes are typically[26] within the range 10^{-4}−10^{-2} mN/m and are therefore much smaller than the area compressibility modulus K_A that has a typical value[29] above 200 mN/m. As a consequence, the area dilations $(A - A_0)/A_0$ are of the order of 10^{-6}−10^{-4} and much too small to be experimentally detectable.

The vesicle−droplet system is thus characterized by three geometric constraints, as provided by the volumes V_α and V_β of the two droplets as well as by the total membrane area A. In order to determine the morphology of the vesicle−droplet system, we will minimize the (free) energy of the system, taking these three constraints into account.

DOI: 10.1021/acs.jpcb.7b10783
J. Phys. Chem. B 2018, 122, 3572−3586

Different Energetic Contributions. The three surface segments and the contact line make different contributions to the total (free) energy of the vesicle−droplet system. One contribution arises from the interfacial tension $\Sigma_{\alpha\beta}$ of the interface between the two liquid phases α and β. The latter contribution is proportional to the interfacial area $A_{\alpha\beta}$ and given by $\Sigma_{\alpha\beta}A_{\alpha\beta}$. The curvature elasticity of each membrane segment $j\gamma$ makes two contributions, a bending energy that depends on the bending rigidity $\kappa_{j\gamma}$ and the spontaneous curvature $m_{j\gamma}$ as well as a contribution from the Gaussian curvature modulus $\kappa_{G,j\gamma}$. When we combine the contributions from both segments, we obtain the bending energy

$$E_{be}^{in} = \sum_{j=\alpha,\beta} 2\kappa_{j\gamma} \int dA_{j\gamma}(M - m_{j\gamma})^2 \tag{1}$$

which depends on the (local) mean curvature M of the membrane, and the Gaussian curvature energy

$$E_G = (\kappa_{G,\alpha\gamma} - \kappa_{G,\beta\gamma}) \oint dl C_g + 2\pi(\kappa_{G,\alpha\gamma} + \kappa_{G,\beta\gamma}) \tag{2}$$

where the first term involves the line integral over the geodesic curvature C_g (see, e.g., ref 30) along the three-phase contact line as follows from the Gauss−Bonnet theorem. To obtain the correct sign of this term, the orientation of the line element dl has to be chosen in such a way that the $\alpha\gamma$ segment is surrounded in a clockwise manner when one looks down onto this segment from the exterior phase γ.

The two energy contributions (1) and (2) correspond to an extension of the spontaneous curvature model[16,17,31] to two distinct membrane segments. In the absence of flip-flops between the two leaflets of the bilayer membrane, the number of membrane molecules is conserved in each bilayer leaflet separately which leads to an additional elastic term that depends on the area difference of the two leaflets.[32,33] On the one hand, the latter term involves additional curvature-elastic parameters that are, in general, difficult to determine. On the other hand, this additional elastic term is irrelevant if the membrane contains (at least) one molecular species such as cholesterol that undergoes frequent flip-flops between the two leaflets. Here, we will focus on such multicomponent membranes and thus ignore contributions from area-difference-elasticity. As emphasized at the beginning of this section, we will also assume that the multicomponent membranes have no tendency to phase separate and have a uniform composition when exposed to a uniform aqueous environment.

Finally, the molecular interactions between the aqueous droplets and the membrane lead to two additional contributions, the adhesion free energies of the droplets and the free energy of the three-phase contact line. The latter contribution is proportional to the length L_{co} of the contact line and given by $L_{co}\lambda_{co}$ with the contact line tension λ_{co}. The adhesion free energies will now be discussed in more detail.

Adhesion Free Energies of Droplets. In order to determine the adhesion free energy of the droplets in contact with the vesicle membrane, we denote the outer and inner leaflet of the bilayer membrane by the subscript "ol" and "il", respectively, and view the leaflet−water interfaces as "walls" with different interfacial tensions, depending on whether they are exposed to the α or to the β phase.

First, let us consider a reference system in which both the α and β droplets have been replaced by the γ phase. The intermolecular interactions between the leaflets and the adjacent γ phases then lead to the interfacial tensions $\Sigma_{ol,\gamma}$ and $\Sigma_{il,\gamma}$ of the corresponding leaflet−water interfaces, and the combined interfacial free energy of both leaflet−water interfaces has the form

$$E_{\gamma\gamma} = (\Sigma_{ol,\gamma} + \Sigma_{il,\gamma})A = (\Sigma_{ol,\gamma} + \Sigma_{il,\gamma})(A_{\alpha\gamma} + A_{\beta\gamma}) \tag{3}$$

We will now make the plausible assumption that we can ignore the dependence of the interfacial tensions on the interfacial curvatures which implies that both leaflet−water interfaces are governed by the same interfacial tension

$$\Sigma_{l\gamma} = \Sigma_{ol,\gamma} = \Sigma_{il,\gamma} \tag{4}$$

corresponding to planar leaflet−water interfaces of a planar bilayer membrane.

If we now go back to the wetting morphology in Figure 1a, the interfacial free energy of the leaflet−water interfaces becomes

$$E_{\alpha\beta} = (\Sigma_{l\alpha} + \Sigma_{l\gamma})A_{\alpha\gamma} + (\Sigma_{l\beta} + \Sigma_{l\gamma})A_{\beta\gamma} \tag{5}$$

The adhesion free energy E_{ad} of the α and the β droplet in contact with one of the leaflets is then defined by

$$E_{ad} \equiv E_{\alpha\beta} - E_{\gamma\gamma} = W_{\alpha\gamma}A_{\alpha\gamma} + W_{\beta\gamma}A_{\beta\gamma} \tag{6}$$

with the adhesion free energies per unit area, $W_{\alpha\gamma}$ and $W_{\beta\gamma}$, given by

$$W_{\alpha\gamma} \equiv \Sigma_{l\alpha} - \Sigma_{l\gamma} \quad \text{and} \quad W_{\beta\gamma} \equiv \Sigma_{l\beta} - \Sigma_{l\gamma} \tag{7}$$

for the α and β droplet, respectively, in contact with one of the membrane leaflets. Because the term "adhesion free energy per unit area" is somewhat clumpsy, I will use the shorter term "adhesive strength" instead. When the leaflet prefers the α phase over the γ phase, the adhesive strength is $W_{\alpha\gamma} < 0$. Likewise, when the leaflet prefers the β phase over the γ phase, $W_{\beta\gamma} < 0$. The adhesive strength $W_{j\gamma}$ also represents the reversible work that has to be expended per unit area to replace the γ phase by the phase j with $j = \alpha, \beta$. In addition, we can also compare the adhesion of the α and β droplets to one of the leaflets without any reference to the γ phase. Thus, the reversible work per unit area to replace the β phase in contact with a leaflet by the α phase is given by

$$W_{\alpha\beta} \equiv \Sigma_{l\alpha} - \Sigma_{l\beta} = W_{\alpha\gamma} - W_{\beta\gamma} \tag{8}$$

If the leaflet prefers the α phase over the β phase, the adhesive strength is $W_{\alpha\beta} < 0$.

Energy Functional for In-Wetting. Now, let us consider any shape S of the vesicle−droplet system with area $A_{\alpha\beta}$ of the water−water interface, areas $A_{\alpha\gamma}$ and $A_{\beta\gamma}$ of the two membrane segments, and length L_{co} of the three-phase contact line. The (free) energy of this shape includes the bending energy E_{be}^{in} and the Gaussian curvature energy E_G as given by (1) and (2) as well as the adhesion free energy E_{ad} in (6). When we collect the different contributions to the energy of the partial in-wetting morphology, we obtain the energy functional

$$\mathcal{E}^{in}\{S\} \equiv \Sigma_{\alpha\beta}A_{\alpha\beta} + E_{be}^{in} + E_G + E_{ad} + \lambda_{co}L_{co} \tag{9}$$

for in-wetting. The superscript "in" indicates that this energy functional corresponds to in-wetting and should be distinguished from out-wetting. In fact, the only energy contribution that is different for in- and out-wetting is the one that arises from the bending energy of the membrane segments because the spontaneous curvatures assume different values when we swap the α and β phases with the γ phase; see further below.

Shape Functional for In-Wetting. In addition to the different energetic contributions of the vesicle−droplet system, we have to take certain constraints on the membrane area A and the droplet volumes V_α and V_β into account. The constraint on

DOI: 10.1021/acs.jpcb.7b10783
J. Phys. Chem. B 2018, 122, 3572−3586

the membrane area A is implemented by the Lagrange multiplier Σ which can be identified with the lateral stress that acts to stretch (or compress) the membrane, as has been explicitly shown for uniform membranes in ref 34. In addition, we have to enforce certain values for the volumes V_α and V_β of the α and β droplets. These volumes are determined by the pressures P_α, P_β, and P_γ within the three liquid phases α, β, and γ or, more precisely, by the pressure differences $P_\alpha - P_\gamma$ and $P_\beta - P_\gamma$. We are then led to study the stationary shapes (minima, maxima, and saddle points) of the shape functional

$$\mathcal{F}^{\text{in}}\{S\} = (P_\gamma - P_\alpha)V_\alpha + (P_\gamma - P_\beta)V_\beta + \Sigma A + \mathcal{E}^{\text{in}}\{S\} \quad (10)$$

where the last term $\mathcal{E}^{\text{in}}\{S\}$ represents the energy functional for in-wetting as given by (9). Both the pressure differences $P_\gamma - P_\alpha$ and $P_\gamma - P_\beta$ as well as the lateral stress Σ will be used as Lagrange multipliers to fulfill the geometric constraints that the droplet volumes V_α and V_β as well as the total membrane area A have certain prescribed values.

Terms Proportional to Individual Segment Areas. The shape functional as given by (10) contains the term ΣA which depends on the lateral membrane stress Σ and the adhesion free energy E_{ad} in (6) which depends on the adhesive strengths of the two aqueous phases. When we combine these two terms, we obtain

$$\Sigma A + E_{\text{ad}} = \Sigma_{\alpha\gamma}A_{\alpha\gamma} + \Sigma_{\beta\gamma}A_{\beta\gamma} \quad (11)$$

with the segment tensions

$$\Sigma_{\alpha\gamma} \equiv \Sigma + W_{\alpha\gamma} \quad \text{and} \quad \Sigma_{\beta\gamma} \equiv \Sigma + W_{\beta\gamma} \quad (12)$$

Thus, each segment tension $\Sigma_{j\gamma}$ depends both on the lateral membrane stress Σ and on the adhesive strength $W_{j\gamma}$. For a given batch of GUVs, the lateral stress Σ depends on the vesicle size and shape and thus varies from vesicle to vesicle. In contrast, the adhesive strength $W_{j\gamma}$ is determined by the molecular interactions across the leaflet–water interfaces and should have the same value for all GUVs from the same batch, assuming that their membranes have the same molecular composition and are exposed to aqueous solutions with the same solute composition. As a consequence, the difference

$$\Sigma_{\alpha\gamma} - \Sigma_{\beta\gamma} = W_{\alpha\gamma} - W_{\beta\gamma} = W_{\alpha\beta} \quad (13)$$

of the two segment tensions is only determined by the adhesive strengths and should also have the same value for all GUVs from the same batch.

SHAPE EQUATIONS AND FORCE BALANCE

Shape Equations for Membrane Segments. The first variation of the shape functional (10) for in-wetting leads to two Euler–Lagrange or shape equations for the two membrane segments $\alpha\gamma$ and $\beta\gamma$, in close analogy to the single shape equation as obtained in ref 35 for the spontaneous curvature model of uniform membranes. The shape equations for the two membrane segments have the form

$$P_j - P_\gamma = 2\Sigma_{j\gamma}M - 2\kappa_{j\gamma}\nabla_{\text{LB}}{}^2M - 4\kappa_{j\gamma}(M - m_{j\gamma}) \times [M(M + m_{j\gamma}) - G] \quad (14)$$

with $j = \alpha, \beta$ and depend, in general, on the (local) mean curvature M and on the (local) Gaussian curvature G of the membrane segments. The $\nabla_{\text{LB}}{}^2$ symbol represents the Laplace–Beltrami operator.[30] For the typical shapes depicted in Figure 1a, the pressure differences $P_\alpha - P_\gamma$ and $P_\beta - P_\gamma$ are positive. Furthermore, the segment tensions $\Sigma_{\alpha\gamma}$ and $\Sigma_{\beta\gamma}$ are given by (12). The shape equations (14) also hold for other curvature models provided one uses an appropriate mapping of the parameters that enter the corresponding shape functionals as shown for uniform membranes in ref 32.

Boundary or Matching Conditions for Axisymmetric Shapes. In addition to the shape equations for the two membrane segments, the first variation of the shape functional also leads to certain boundary or matching conditions for the curvatures of the two segments along the contact line. For axisymmetric vesicles as depicted in Figure 2, these matching conditions

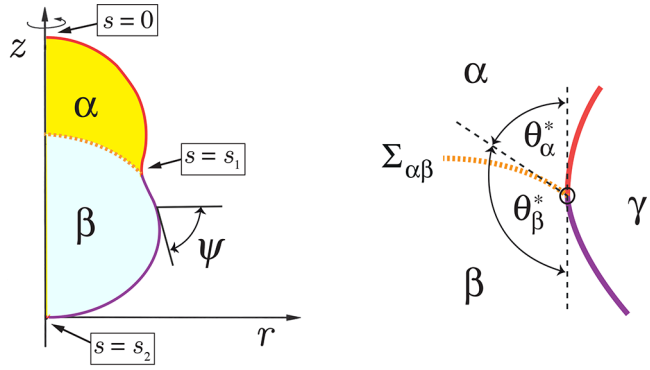

Figure 2. (a) Axisymmetric shape corresponding to partial in-wetting: The two-dimensional shape is uniquely determined by the one-dimensional shape contour (red-purple) in the (r, z)-plane defined by the coordinate z along the symmetry axis and the radial coordinate r. The shape contour is parametrized by its arc length s, with the north and south poles of the vesicle being located at $s = 0$ and $s = s_2$, respectively, and the contact line at $s = s_1$. The angle ψ describes the tilt of the tangent vector at the shape contour from the horizontal r-direction. (b) The $\alpha\gamma$ segment (red) and the $\beta\gamma$ segment (purple) meet at the contact line with a common tangent. The angles between this tangent and the tangent to the $\alpha\beta$ interface (dashed orange) represent the intrinsic contact angles θ_α^* and θ_β^* with $\theta_\alpha^* + \theta_\beta^* = \pi$.

can be obtained by generalizing the corresponding conditions for two-domain vesicles.[31]

The shape of an axisymmetric vesicle is uniquely determined by the symmetry axis and the shape contour. In Figure 2, the symmetry axis is provided by the z-axis. We could then use cylindrical coordinates, r and z, to describe the vesicle shape, but it is more convenient to parametrize the contour in terms of its arc length s and to use the radial coordinate r as well as the tilt angle ψ as defined in Figure 2a. The north pole of the shape is located at $s = 0$, the south pole at $s = s_2$, and the contact line at $s = s_1$.

The two principal curvatures of the membrane shape are then given by the contour curvature $C_1(s) = \mathrm{d}\psi/\mathrm{d}s$ and the orthogonal curvature $C_2(s) = \sin\psi/r$. In general, the contour curvature C_1 attains two different values, $C_1(s_1 - \epsilon)$ and $C_1(s_1 + \epsilon)$, when we approach the contact line from the $\alpha\gamma$ and $\beta\gamma$ segments, respectively, while the orthogonal curvature C_2 is continuous across the contact line. The first variation of the shape functional with respect to the variable $\psi(s_1)$ leads to the discontinuity

$$\kappa_{\beta\gamma}C_1(s_1 + \epsilon) - \kappa_{\alpha\gamma}C_1(s_1 - \epsilon) = \delta\kappa C_2(s_1) + 2\kappa_{\beta\gamma}m_{\beta\gamma} - 2\kappa_{\alpha\gamma}m_{\alpha\gamma} \quad (15)$$

of the contour curvature C_1 with the parameter

$$\delta\kappa \equiv \kappa_{\alpha\gamma} - \kappa_{\beta\gamma} + \kappa_{\text{G},\alpha\gamma} - \kappa_{\text{G},\beta\gamma} \quad (16)$$

DOI: 10.1021/acs.jpcb.7b10783
J. Phys. Chem. B 2018, 122, 3572–3586

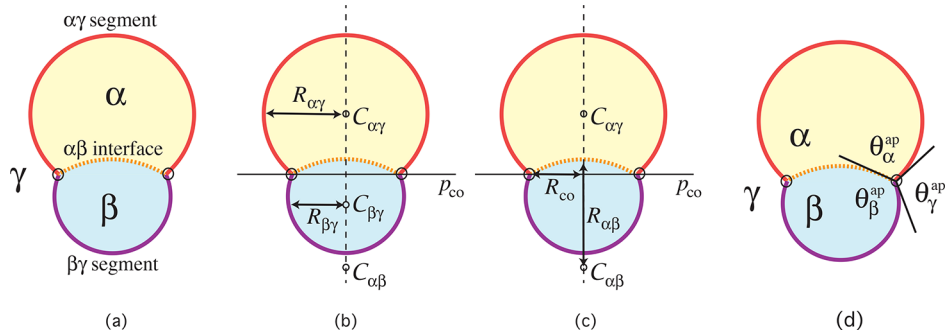

Figure 3. Cross section of partial in-wetting morphology as observed experimentally: (a) Three spherical surface segments corresponding to the $\alpha\beta$ interface (orange) and to the two membrane segments $\alpha\gamma$ (red) and $\beta\gamma$ (purple). These three spherical caps meet along an apparent contact line (black circles). (b, c) The three-spherical-cap shape is determined by the three curvature radii $R_{\alpha\gamma}$, $R_{\beta\gamma}$, and $R_{\alpha\beta}$ as well as by the contact line radius R_{co}. The three centers $C_{\alpha\gamma}$, $C_{\beta\gamma}$, and $C_{\alpha\beta}$ of the three spherical caps are located on the rotational symmetry axis (vertical dashed line). In order to obtain a unique shape, we also need to specify the locations of these cap centers relative to the contact line plane p_{co} (full horizontal line); see main text. (d) At the contact line, the tangent planes to the three spherical surface segments define the three apparent contact angles θ_α^{ap}, θ_β^{ap}, and θ_γ^{ap} with $\theta_\alpha^{ap} + \theta_\beta^{ap} + \theta_\gamma^{ap} = 2\pi$.

Note that the individual contour curvatures $C_1(s_1 + \epsilon)$ and $C_1(s_1 - \epsilon)$ are usually quite large compared to the orthogonal curvature $C_2(s_1)$ that satisfies $C_2(s_1) = \sin\psi(s_1)/r(s_1) \leq 1/r(s_1)$. The discontinuity $C_1(s_1 + \epsilon) - C_1(s_1 - \epsilon)$ of the contour curvature vanishes if the two membrane segments have the same curvature-elastic properties, i.e., the same spontaneous curvature, bending rigidity, and Gaussian curvature modulus. The latter situation applies in particular to the case $m_{\alpha\gamma} = m_{\beta\gamma} = 0$ studied in ref 24.

Balance between Interfacial and Segment Tensions. A second boundary or matching condition is obtained from the first variation of the shape functional with respect to the variable $r_1 \equiv r(s_1)$ which represents the radius of the contact line. The latter variation leads to

$$\Sigma_{\beta\gamma} - \Sigma_{\alpha\gamma} = \Sigma_{\alpha\beta}\cos\theta_\alpha^* + \lambda_{co}\frac{\cos\psi_1}{r_1} + \Delta_{\Sigma,co} \tag{17}$$

with $\psi_1 \equiv \psi(s_1)$. The last term in (17) has the explicit form

$$\Delta_{\Sigma,co} = \frac{1}{2}\kappa_{\beta\gamma}Q_{\beta\gamma}(s_1 + \epsilon) - \frac{1}{2}\kappa_{\alpha\gamma}Q_{\alpha\gamma}(s_1 - \epsilon) \tag{18}$$

with the curvature-dependent terms

$$Q_{j\gamma}(s) \equiv C_1^2(s) - [C_2(s) - 2m_{j\gamma}]^2 \quad \text{for} \quad j = \alpha, \beta \tag{19}$$

These relations describe the balance between the capillary forces arising from the interfacial tension $\Sigma_{\alpha\beta}$, the tensions $\Sigma_{\beta\gamma}$ and $\Sigma_{\alpha\gamma}$ of the two membrane segments, and the line tension λ_{co}. The additional term $\Delta_{\Sigma,co}$ in (17) arises from the different curvature-elastic properties of the two membrane segments. Indeed, the term $\Delta_{\Sigma,co}$ vanishes if the two membrane segments have the same curvature-elastic properties. In the latter case, we obtain from (17) and (13) that

$$\Sigma_{\beta\gamma} - \Sigma_{\alpha\gamma} = W_{\beta\gamma} - W_{\alpha\gamma} = \Sigma_{\alpha\beta}\cos\theta_\alpha^* + \lambda_{co}\frac{\cos\psi_1}{r_1} \tag{20}$$

which depends on the adhesion strengths $W_{\beta\gamma}$ and $W_{\alpha\gamma}$ of the two membrane segments, the interfacial tension $\Sigma_{\alpha\beta}$, and the contact line tension λ_{co}. Thus, if the vesicle membrane continued to have uniform curvature-elastic properties even when it is partially wetted by the two aqueous droplets, the force balance (20) along the contact line would involve neither the bending rigidity nor the spontaneous curvature of the membrane. For GUVs, the radius r_1 of the contact line is typically of the order of many micrometers. In such a situation, the term proportional to the line tension λ_{co} in (20) can be neglected, which implies that the intrinsic contact angle θ_α^* depends only on three material parameters, the adhesive strengths $W_{\beta\gamma}$ and $W_{\alpha\gamma}$ as well as the interfacial tension $\Sigma_{\alpha\beta}$ of the water−water interface.

If the two membrane segments have different spontaneous curvatures but the same bending rigidities κ and the same Gaussian curvature moduli, the additional term $\Delta_{\Sigma,co}$ becomes

$$\Delta_{\Sigma,co} = 4\kappa[m_{\beta\gamma} - m_{\alpha\gamma}][M(s_1 - \epsilon) - m_{\alpha\gamma}] \tag{21}$$

with the mean curvature $M = \frac{1}{2}(C_1 + C_2)$ which satisfies, for $\kappa_{\alpha\gamma} = \kappa_{\beta\gamma} = \kappa$ and $\kappa_{G,\alpha\gamma} = \kappa_{G,\beta\gamma}$, the matching condition

$$M(s_1 + \epsilon) - m_{\beta\gamma} = M(s_1 - \epsilon) - m_{\alpha\gamma} \tag{22}$$

along the contact line as follows from (15). Thus, the discontinuity in the mean curvature, $M(s_1 + \epsilon) - M(s_1 - \epsilon)$, is now equal to the difference in the spontaneous curvatures, $m_{\beta\gamma} - m_{\alpha\gamma}$, and the additional term $\Delta_{\Sigma,co}$ is proportional to this discontinuity.

At present, both the curvature discontinuities and the additional term $\Delta_{\Sigma,co}$ that enters the force balance relation (17) cannot be used to analyze the shapes of GUVs because the local membrane curvatures along the contact line are not resolved by optical microscopy. Therefore, these matching conditions will not be further pursued in the following. On the other hand, the experimental observations revealed one universal feature of the partial wetting morphologies for GUVs, namely, that the shapes of the two membrane segments are very well described by spherical caps which is a direct consequence of the capillary forces exerted by the $\alpha\beta$ interface onto the vesicle membrane. Because the $\alpha\beta$ interface necessarily forms a spherical cap as follows from the classical Laplace equation, the partial wetting morphologies consist of three surface segments that form three spherical caps and meet along the three-phase contact line; see Figure 3a.

THREE SPHERICAL CAPS: GEOMETRIC RELATIONS

Geometry of Three-Spherical-Cap Shapes. From the optical microscopy images, we can directly deduce the curvature radii of the three spherical caps which will be denoted by $R_{\alpha\beta}$, $R_{\alpha\gamma}$, and $R_{\beta\gamma}$, respectively, see Figure 3b,c, and the centers of the spherical caps by $C_{\alpha\gamma}$, $C_{\beta\gamma}$, and $C_{\alpha\beta}$. We will use the sign convention that all radii are always taken to be positive. Because the three spherical caps meet along a common contact line, the three cap centers $C_{\alpha\gamma}$, $C_{\beta\gamma}$, and $C_{\alpha\beta}$ are necessarily colinear. The straight line through these centers represents the axis of rotational symmetry for the three-spherical-cap shape corresponding to

DOI: 10.1021/acs.jpcb.7b10783
J. Phys. Chem. B 2018, 122, 3572−3586

the vertical dashed line in Figure 3b,c. To obtain a certain three-spherical-cap shape, we also need to specify the radius R_{co} of the apparent contact line in addition to the curvature radii; see Figure 3c. In fact, the four length scales $R_{\alpha\beta}$, $R_{\alpha\gamma}$, $R_{\beta\gamma}$, and R_{co} are not quite sufficient to uniquely define the three-spherical-cap shape because we still need to specify whether the $\alpha\beta$ interface bulges toward the α or toward the β droplet.

In Figure 3, the α-rich and β-rich droplets are located above and below the contact line plane p_{co} corresponding to the full horizontal line. In addition, the center $C_{\alpha\beta}$ of the $\alpha\beta$ interface is located below the plane p_{co} which implies that the $\alpha\beta$ interface bulges toward the α droplet corresponding to a pressure P_β in the β droplet that exceeds the pressure P_α in the α droplet. Keeping the four length scales fixed as well as the locations of the two cap centers $C_{\alpha\gamma}$ and $C_{\beta\gamma}$, we may also locate the center $C_{\alpha\beta}$ on top of the contact line plane p_{co} which then leads to an $\alpha\beta$ interface that bulges toward the β droplet corresponding to $P_\alpha > P_\beta$.

We now introduce the sign convention that the mean curvature $M_{\alpha\beta}$ of the $\alpha\beta$ interface is *positive*, i.e.,

$$M_{\alpha\beta} = \frac{1}{R_{\alpha\beta}} > 0 \quad \text{for} \quad P_\alpha > P_\beta \tag{23}$$

and *negative* with

$$M_{\alpha\beta} = -\frac{1}{R_{\alpha\beta}} < 0 \quad \text{for} \quad P_\beta > P_\alpha \tag{24}$$

With this sign convention, the classical Laplace equation for the $\alpha\beta$ interface assumes the form

$$P_\alpha - P_\beta = 2\Sigma_{\alpha\beta}M_{\alpha\beta} = \pm\frac{2\Sigma_{\alpha\beta}}{R_{\alpha\beta}} \tag{25}$$

where the plus and minus sign corresponds to $P_\alpha > P_\beta$ and $P_\beta > P_\alpha$, respectively.

Family of Three-Spherical-Cap Shapes with Geometric Constraints. As explained at the beginning of the last section, the vesicle−droplet systems are characterized by three geometric constraints as provided by the droplet volumes V_α and V_β as well as by the total membrane area A. These three quantities can be expressed in terms of the four radii $R_{\alpha\beta}$, $R_{\alpha\gamma}$, $R_{\beta\gamma}$, and R_{co} which leads to three equations between the four radii. The solution of these three equations may be parametrized in terms of V_α, V_β, A, and a suitable reaction coordinate such as the contact line radius R_{co}, which then provides a one-parameter family of three-spherical-cap shapes that fulfill all three geometric constraints.

Apparent Contact Angles. Another set of geometric quantities that can be directly deduced from the optical microscopy images are the apparent contact angles θ_α^{ap}, θ_β^{ap}, and θ_γ^{ap}, with $\theta_\alpha^{ap} + \theta_\beta^{ap} + \theta_\gamma^{ap} = 2\pi$; see Figure 3d. These angles can be expressed in terms of the three curvature radii and the contact line radius R_{co}. For the case displayed in Figure 3, one then obtains the explicit relations

$$\sin\theta_\alpha^{ap} = \frac{R_{co}}{R_{\alpha\gamma}R_{\alpha\beta}}\left(\sqrt{R_{\alpha\gamma}^2 - R_{co}^2} + \sqrt{R_{\alpha\beta}^2 - R_{co}^2}\right) \tag{26}$$

$$\sin\theta_\beta^{ap} = \frac{R_{co}}{R_{\alpha\beta}R_{\beta\gamma}}\left(\sqrt{R_{\alpha\beta}^2 - R_{co}^2} - \sqrt{R_{\beta\gamma}^2 - R_{co}^2}\right) \tag{27}$$

with $R_{\alpha\beta} \geq R_{\beta\gamma}$ and

$$\sin\theta_\gamma^{ap} = \frac{R_{co}}{R_{\alpha\gamma}R_{\beta\gamma}}\left(\sqrt{R_{\alpha\gamma}^2 - R_{co}^2} + \sqrt{R_{\beta\gamma}^2 - R_{co}^2}\right) \tag{28}$$

Angle−Curvature Relationship. Finally, using some trigonometric relations, it is not difficult to show that the curvature radii and the apparent contact angles satisfy the relation

$$\mp\frac{\sin\theta_\gamma^{ap}}{R_{\alpha\beta}} = \frac{\sin\theta_\alpha^{ap}}{R_{\beta\gamma}} - \frac{\sin\theta_\beta^{ap}}{R_{\alpha\gamma}} \tag{29}$$

where the minus and plus sign applies to an $\alpha\beta$ interface that bulges toward the β and the α droplet, respectively. The equalities in (29), which do not depend on the contact line radius R_{co}, may be used to estimate the accuracy of the measured values for the curvature radii and apparent contact angles. When expressed in terms of the mean curvatures, the purely geometric relation (29) becomes

$$M_{\alpha\beta}\sin\theta_\gamma^{ap} = M_{\alpha\gamma}\sin\theta_\beta^{ap} - M_{\beta\gamma}\sin\theta_\alpha^{ap} \tag{30}$$

THREE SPHERICAL CAPS: SHAPE EQUATIONS

Shape Equations for Spherical Membrane Segments. When the membrane segments $\alpha\gamma$ and $\beta\gamma$ assume spherical cap shapes, the shape equations (14) assume the simplified form

$$P_j - P_\gamma = 2\Sigma_{j\gamma}M_{j\gamma} + 4\kappa_{j\gamma}m_{j\gamma}^2M_{j\gamma} - 4\kappa_{j\gamma}m_{j\gamma}M_{j\gamma}^2 \quad \text{with} \quad j = \alpha, \beta \tag{31}$$

which can be rewritten as

$$P_j - P_\gamma = 2\Sigma_{j\gamma}^{eff}M_{j\gamma} \quad \text{for} \quad j = \alpha, \beta \tag{32}$$

with the effective tensions defined by

$$\Sigma_{j\gamma}^{eff} \equiv \Sigma_{j\gamma} + 2\kappa_{j\gamma}m_{j\gamma}(m_{j\gamma} - M_{j\gamma}) \tag{33}$$

Note that these shape equations now determine the *constant* mean curvatures $M_{\alpha\gamma}$ and $M_{\beta\gamma}$ of the two spherical membrane segments.

The second term on the right-hand side of (33) represents the spontaneous tensions[28]

$$\sigma_{j\gamma} \equiv 2\kappa_{j\gamma}m_{j\gamma}^2 \tag{34}$$

which are the natural tension scales for the two membrane segments. Using the decomposition (12) for the segment tensions $\Sigma_{j\gamma}$, the effective tensions $\Sigma_{j\gamma}^{eff}$ become

$$\Sigma_{j\gamma}^{eff} \equiv \Sigma + W_{j\gamma} + \sigma_{j\gamma} - 2\kappa_{j\gamma}m_{j\gamma}M_{j\gamma} \tag{35}$$

with the lateral membrane stress Σ, the adhesive strengths $W_{j\gamma}$, and the spontaneous tensions $\sigma_{j\gamma}$.

A linear combination of the Laplace equation (25) for the $\alpha\beta$ interface and the shape equations (32) for the two membrane segments can be used to eliminate the three pressure differences. As a result, we obtain the relation

$$\Sigma_{\alpha\beta}M_{\alpha\beta} = \Sigma_{\alpha\gamma}^{eff}M_{\alpha\gamma} - \Sigma_{\beta\gamma}^{eff}M_{\beta\gamma} \tag{36}$$

between the interfacial tension $\Sigma_{\alpha\beta}$ and the effective tensions $\Sigma_{\alpha\gamma}^{eff}$ and $\Sigma_{\beta\gamma}^{eff}$ experienced by the two membrane segments.

Relationships between Tensions, Contact Angles, and Curvatures. Using a combination of the geometric relation (30) and the curvature−tension relation (36), we can now eliminate the mean curvature $M_{\alpha\beta}$ of the $\alpha\beta$ interface which leads to the relationship

$$M_{\alpha\gamma}\left(\frac{\Sigma_{\alpha\gamma}^{eff}}{\Sigma_{\alpha\beta}} - \frac{\sin\theta_\beta^{ap}}{\sin\theta_\gamma^{ap}}\right) = M_{\beta\gamma}\left(\frac{\Sigma_{\beta\gamma}^{eff}}{\Sigma_{\alpha\beta}} - \frac{\sin\theta_\alpha^{ap}}{\sin\theta_\gamma^{ap}}\right) \tag{37}$$

DOI: 10.1021/acs.jpcb.7b10783
J. Phys. Chem. B 2018, 122, 3572−3586

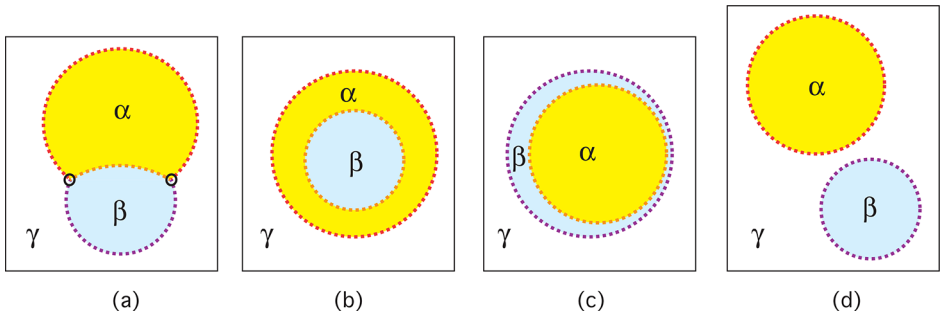

Figure 4. Wetting morphologies for two liquid droplets composed of the aqueous phases α (yellow) and β (blue), both of which coexist with the bulk liquid phase γ (white): (a) Partial wetting of the three phases which leads to a three-phase contact line (black circles); (b) complete wetting of the $\beta\gamma$ interface by the α phase; (c) complete wetting of the $\alpha\gamma$ interface by the β phase; and (d) complete wetting of the $\alpha\beta$ interface by the γ phase.

between the effective tensions, the apparent contact angles, and the mean curvatures of the $\alpha\gamma$ and $\beta\gamma$ membrane segments. It is important to note that the derivation of (37) was based (i) on the purely geometric relation (30) which applies to three spherical caps that intersect along a common contact line and (ii) on the shape equations for the spherical membrane segments and the $\alpha\beta$ interface. In particular, this derivation did not make any assumptions about the mechanical balance of the interfacial and membrane tensions along the contact line.

Digression: Droplets without Vesicle. It is instructive to briefly consider the related but somewhat different wetting morphologies corresponding to two liquid droplets composed of the aqueous phases α and β, both of which coexist with the bulk liquid phase γ as depicted in Figure 4 in the absence of the vesicle. The latter system is characterized by the three interfacial tensions $\Sigma_{\alpha\beta}$, $\Sigma_{\alpha\gamma}$, and $\Sigma_{\beta\gamma}$. Comparison with the in-wetting morphologies of GUVs as shown in Figure 1 reveals that the two-droplet morphologies in Figure 4 can be obtained from those in Figure 1 by simply removing the vesicle membrane.

Using the same line of reasoning as for GUVs, we then obtain the relationship

$$M_{\alpha\gamma}\left(\frac{\Sigma_{\alpha\gamma}}{\Sigma_{\alpha\beta}}-\frac{\sin\theta_\beta}{\sin\theta_\gamma}\right)=M_{\beta\gamma}\left(\frac{\Sigma_{\beta\gamma}}{\Sigma_{\alpha\beta}}-\frac{\sin\theta_\alpha}{\sin\theta_\gamma}\right) \tag{38}$$

for the partial wetting morphology of two droplets in the absence of the vesicle membrane. The latter relationship has the same form as the relationship (37) for partial in-wetting of GUVs. However, in contrast to the effective tensions $\Sigma^{\mathrm{eff}}_{j\gamma}$ in (37), the interfacial tensions in (38) represent material parameters that do not depend on the size of the droplets. Furthermore, for large droplet sizes, the contact angles θ_α, θ_β, and θ_γ should not depend on the droplet sizes either. We can then conclude that the two parentheses in (38) enclose expressions that are independent of the droplet size. On the other hand, changes in the droplet shape obvioulsy change the mean curvatures $M_{\alpha\gamma}=1/R_{\alpha\gamma}$ and $M_{\beta\gamma}=1/R_{\beta\gamma}$. Therefore, the relation (38) can only hold in general if the expressions in the two parentheses vanish separately, i.e., if

$$\frac{\Sigma_{\alpha\gamma}}{\Sigma_{\alpha\beta}}=\frac{\sin\theta_\beta}{\sin\theta_\gamma}\quad\text{and}\quad\frac{\Sigma_{\beta\gamma}}{\Sigma_{\alpha\beta}}=\frac{\sin\theta_\alpha}{\sin\theta_\gamma} \tag{39}$$

which relate the interfacial tensions to the contact angles. The latter relations are equivalent to

$$\frac{\Sigma_{\alpha\beta}}{\sin\theta_\gamma}=\frac{\Sigma_{\alpha\gamma}}{\sin\theta_\beta}=\frac{\Sigma_{\beta\gamma}}{\sin\theta_\alpha} \tag{40}$$

which represent the law of sines for a triangle, the sides of which are formed by the three interfacial tensions. In the context of interfacial wetting, the latter triangle is known as Neumann's triangle.[15]

Size Dependence of Effective Tensions and Apparent Contact Angles. Let us now return to the partial in-wetting morphologies of GUVs and to the general relationship (37) for the two membrane segments. In this case, the two expressions in parentheses are expected to depend on the geometry of the vesicle−droplet system in a complicated manner. First, the apparent contact angles depend on the volumes V_α and V_β, as observed experimentally in ref 24. Second, the effective tensions $\Sigma^{\mathrm{eff}}_{j\gamma}$ as given by (35) also depend on the geometry, both via the overall membrane stress Σ and via the terms proportional to $M_{j\gamma}=1/R_{j\gamma}$. Because of these dependencies, the two parentheses in the relationship (37) do not have to vanish separately. However, we can still obtain useful relations from (37) if we consider GUVs for which the mean curvatures $M_{\alpha\gamma}$ and $M_{\beta\gamma}$ fulfill certain conditions and/or if the overall membrane stress is small and can be neglected.

Indeed, the relationship (37) becomes

$$\frac{\Sigma^{\mathrm{eff}}_{\alpha\gamma}}{\Sigma_{\alpha\beta}}\approx\frac{\sin\theta^{\mathrm{ap}}_\beta}{\sin\theta^{\mathrm{ap}}_\gamma}\quad\text{for small } M_{\beta\gamma}/M_{\alpha\gamma} \tag{41}$$

and

$$\frac{\Sigma^{\mathrm{eff}}_{\beta\gamma}}{\Sigma_{\alpha\beta}}\approx\frac{\sin\theta^{\mathrm{ap}}_\alpha}{\sin\theta^{\mathrm{ap}}_\gamma}\quad\text{for small } M_{\alpha\gamma}/M_{\beta\gamma} \tag{42}$$

Furthermore, the relationship (37) assumes the form

$$\frac{\Sigma^{\mathrm{eff}}_{\alpha\gamma}-\Sigma^{\mathrm{eff}}_{\beta\gamma}}{\Sigma_{\alpha\beta}}=\frac{\sin\theta^{\mathrm{ap}}_\beta-\sin\theta^{\mathrm{ap}}_\alpha}{\sin\theta^{\mathrm{ap}}_\gamma}\quad\text{for}\quad M_{\alpha\gamma}=M_{\beta\gamma} \tag{43}$$

The latter relation, which is independent of the overall lateral stress Σ, does not require that the volumes V_α and V_β are roughly equal. Indeed, GUVs with $M_{\alpha\gamma}\simeq M_{\beta\gamma}$ have been previously observed[20,24] when the total volume $V=V_\alpha+V_\beta$ was close to the volume of a sphere with surface area $A=A_{\alpha\gamma}+A_{\beta\gamma}$.

Another special case is obtained for a planar $\alpha\beta$ interface with $M_{\alpha\beta}=0$. In this case, the two relations (36) and (30) lead to $M_{\beta\gamma}/M_{\alpha\gamma}=\Sigma^{\mathrm{eff}}_{\alpha\gamma}/\Sigma^{\mathrm{eff}}_{\beta\gamma}$ and $M_{\beta\gamma}/M_{\alpha\gamma}=\sin\theta^{\mathrm{ap}}_\beta/\sin\theta^{\mathrm{ap}}_\alpha$, which implies

$$\frac{\Sigma^{\mathrm{eff}}_{\alpha\gamma}}{\Sigma^{\mathrm{eff}}_{\beta\gamma}}=\frac{\sin\theta^{\mathrm{ap}}_\beta}{\sin\theta^{\mathrm{ap}}_\alpha}\quad\text{for}\quad M_{\alpha\beta}=0 \tag{44}$$

DOI: 10.1021/acs.jpcb.7b10783
J. Phys. Chem. B 2018, 122, 3572−3586

The four relations (41)−(44) can be used to analyze different GUVs from the same batch which are formed by membranes with the same lipid composition and are exposed to aqueous two-phase systems with the same solute and polymer concentrations. What we would like to do in particular is to use these relations to estimate the material parameters of the vesicle−droplet systems.

Material Parameters of Vesicle−Droplet Systems. The left-hand sides of the relations (41)−(44) depend on the effective tensions $\Sigma_{j\gamma}^{\mathrm{eff}}$ and on the interfacial tension $\Sigma_{\alpha\beta}$. The interfacial tension represents a material parameter that can be measured independently by studying macroscopic interfaces between two bulk phases α and β, as has been done for PEG−dextran solutions in ref 12. In addition, the effective tensions $\Sigma_{\alpha\gamma}^{\mathrm{eff}}$ as given by (35) can be rewritten in the form

$$\Sigma_{j\gamma}^{\mathrm{eff}} = \Sigma + X_{j\gamma} + Y_{j\gamma} M_{j\gamma} \tag{45}$$

with the material parameters

$$X_{j\gamma} \equiv W_{j\gamma} + \sigma_{j\gamma} \quad \text{and} \quad Y_{j\gamma} \equiv -2\kappa_{j\gamma} m_{j\gamma} \tag{46}$$

When we insert these expressions for the effective tensions $\Sigma_{j\gamma}^{\mathrm{eff}}$ into the relationships (41)−(43), we see that these relationships contain three different types of quantities: (i) the mean curvatures of the spherical membrane segments and the apparent contact angles, two types of geometric quantities that can be directly deduced from the microscopy images; (ii) the material parameters $X_{j\gamma}$ and $Y_{j\gamma}$; and (iii) the lateral membrane stress Σ that depends on the size and shape of the GUVs and represents a hidden variable from the experimental point of view.

The adhesive strengths are governed by the molecular interactions across the leaflet−water interfaces. Likewise, the spontaneous curvatures and spontaneous tensions are generated by the molecular asymmetry between these two leaflets. Both the adhesive strengths $W_{j\gamma}$ and the spontaneous tensions $\sigma_{j\gamma}$ will hardly change when the GUVs are slightly deflated. In contrast, the lateral stress Σ will be strongly reduced even by small deflation steps. Thus, using such a deflation step, we should be able to obtain effective tensions that are well approximated by

$$\Sigma_{j\gamma,0}^{\mathrm{eff}} \equiv X_{j\gamma} + Y_{j\gamma} M_{j\gamma} \tag{47}$$

In such a situation, we can deduce the values of $X_{\alpha\gamma} = W_{\alpha\gamma} + \sigma_{\alpha\gamma}$ and $Y_{\alpha\gamma} = -2\kappa_{\alpha\gamma} m_{\alpha\gamma}$ by applying the relationship (41) to two GUVs with different values of $M_{\alpha\gamma}$, both of which are large compared to $M_{\beta\gamma}$. Likewise, we can deduce the values of $X_{\beta\gamma} = W_{\beta\gamma} + \sigma_{\beta\gamma}$ and $Y_{\beta\gamma} = -2\kappa_{\beta\gamma} m_{\beta\gamma}$ by applying the relationship (42) to two GUVs with different values of $M_{\beta\gamma}$, both of which are large compared to $M_{\alpha\gamma}$. The values for $X_{j\gamma}$ and $Y_{j\gamma}$ obtained in this way can be cross-checked and scrutinized by examining (i) additional GUVs with $M_{\beta\gamma} \ll M_{\alpha\gamma}$ and (ii) additional GUVs with $M_{\beta\gamma} \gg M_{\alpha\gamma}$ as well as (iii) by selecting vesicles for which we can use the relationships (43) and (44).

Furthermore, when we assume the typical value $\kappa_{j\gamma} \simeq 10^{-19}$ J for the bending ridigities of the two membrane segments, we obtain rough estimates for the spontaneous curvatures $m_{j\gamma}$ and the spontaneous tensions $\sigma_{j\gamma}$ from the values of $Y_{j\gamma}$. Finally, we can deduce the values of the adhesive strengths $W_{j\gamma}$ from the values of $\sigma_{j\gamma}$ and $X_{j\gamma}$. In this way, the relationships (41)−(44) lead to estimates for all material parameters of the vesicle−droplet systems.

Regime of Small Lateral Stress. As described in the previous paragraph, osmotic deflation could be used to obtain GUVs with a small lateral stress Σ. If we can ignore this overall membrane stress, the general relationship (37) becomes

$$M_{\alpha\gamma}\bar{X}_{\alpha\gamma} + M_{\alpha\gamma}{}^2\bar{Y}_{\alpha\gamma} - M_{\beta\gamma}\bar{X}_{\beta\gamma} - M_{\beta\gamma}{}^2\bar{Y}_{\beta\gamma} = \Xi \tag{48}$$

with the variables

$$\bar{X}_{j\gamma} \equiv \frac{X_{j\gamma}}{\Sigma_{\alpha\beta}} \quad \text{and} \quad \bar{Y}_{j\gamma} \equiv \frac{Y_{j\gamma}}{\Sigma_{\alpha\beta}} \tag{49}$$

as well as the experimentally accessible curvature

$$\Xi \equiv M_{\alpha\gamma}\frac{\sin\theta_\beta^{\mathrm{ap}}}{\sin\theta_\gamma^{\mathrm{ap}}} - M_{\beta\gamma}\frac{\sin\theta_\alpha^{\mathrm{ap}}}{\sin\theta_\gamma^{\mathrm{ap}}} \tag{50}$$

The relationship (48) contains the four unknowns $\bar{X}_{\alpha\gamma}$, $\bar{Y}_{\alpha\gamma}$, $\bar{X}_{\beta\gamma}$, and $\bar{Y}_{\beta\gamma}$. In order to determine these four unknowns, we need (at least) four equations of the form (48); i.e., we need to determine the two spherical cap radii $R_{j\gamma} = 1/M_{j\gamma}$ and the three apparent contact angles for (at least) four GUVs from the same batch.

Several Droplets Adhering to the Same GUV. As previously emphasized, the overall lateral stress Σ within the vesicle membrane cannot be directly measured but depends on the preparation of the vesicle and varies, in general, from vesicle to vesicle. Therefore, in the two preceding subsections, we assumed osmotic conditions for which the contribution of Σ to the effective membrane tensions $\Sigma_{j\gamma}^{\mathrm{eff}}$ as defined by (35) can be neglected. This assumption becomes unnecessary if we observe several α or several β droplets in contact with the same vesicle membrane.

Thus, consider a situation in which several α droplets adhere to the interior leaflet of the same GUV membrane. These droplets are in contact with one large β droplet inside the GUV. The different α droplets are labeled by $n = 1, 2, \ldots, N$. The vesicle membrane is then partitioned into $N + 1$ segments labeled by $n\gamma$ and $\beta\gamma$. The different $n\gamma$ segments experience the effective membrane tensions

$$\Sigma_{\alpha\gamma}^{(n)} = \Sigma + W_{\alpha\gamma} + \sigma_{\alpha\gamma} - 2\kappa_{\alpha\gamma} m_{\alpha\gamma} M_{\alpha\gamma}^{(n)} \tag{51}$$

where all parameters on the right-hand side are independent of n apart from the mean curvatures $M_{\alpha\gamma}^{(n)}$ of the $n\gamma$ segments. In addition, the apparent contact line of the α droplet n can be characterized by the apparent contact angles $\theta_\alpha^{(n)}$, $\theta_\beta^{(n)}$, and $\theta_\gamma^{(n)}$. For such a geometry, we obtain N relationships of the form

$$\Upsilon_{\alpha\gamma}^{(n)} \equiv M_{\alpha\gamma}^{(n)}\left(\frac{\Sigma_{\alpha\gamma}^{(n)}}{\Sigma_{\alpha\beta}} - \frac{\sin\theta_\beta^{(n)}}{\sin\theta_\gamma^{(n)}}\right) + M_{\beta\gamma}\frac{\sin\theta_\alpha^{(n)}}{\sin\theta_\gamma^{(n)}} = M_{\beta\gamma}\frac{\Sigma_{\beta\gamma}^{\mathrm{eff}}}{\Sigma_{\alpha\beta}} \tag{52}$$

with $n = 1, 2, \ldots, N$. This set of equations implies that

$$\Upsilon_{\alpha\gamma}^{(1)} = \Upsilon_{\alpha\gamma}^{(2)} = \ldots = \Upsilon_{\alpha\gamma}^{(N)} \tag{53}$$

Therefore, from three different $n\gamma$ segments with three distinct mean curvatures $M_{\alpha\gamma}^{(n)}$ and, thus, three distinct expressions $\Upsilon_{\alpha\gamma}^{(n)}$, we obtain two linearly independent equations from which we can deduce the two parameter combinations $(\Sigma + W_{\alpha\gamma} + \sigma_{\alpha\gamma})/\Sigma_{\alpha\beta}$ and $\kappa_{\alpha\gamma} m_{\alpha\gamma}/\Sigma_{\alpha\beta}$ for any value of Σ.

THREE SPHERICAL CAPS: FORCE BALANCE

As shown in Figure 3, the geometry of three spherical caps that meet at a common contact line can be parametrized by the three curvature radii $R_{\alpha\beta}$, $R_{\alpha\gamma}$, and $R_{\beta\gamma}$, as well as by the contact line radius R_{co}. In the previous section, we combined the purely

DOI: 10.1021/acs.jpcb.7b10783
J. Phys. Chem. B 2018, 122, 3572−3586

geometric relation (29) for the three-spherical cap shapes with (i) the classical Laplace equation (25) for the curvature radius $R_{\alpha\beta}$ of the $\alpha\beta$ interface and (ii) the shape equations (32) for the curvature radii $R_{\alpha\gamma}$ and $R_{\beta\gamma}$ of the two membrane segments. The resulting relationships (37) as well as (52) and (53) were derived without any use of the contact line radius R_{co}.

In the present section, we will describe a somewhat different approach, starting from the energy functional $\mathcal{E}^{in}\{S\}$ and the shape functional $\mathcal{F}^{in}\{S\}$, as given by (9) and (10) and applying these functionals to the three-spherical-cap shapes $S = S_{sc}$. The energy functional then assumes the form

$$\mathcal{E}^{in}_{sc} \equiv \mathcal{E}^{in}\{S_{sc}\} = E^{in}_{sc}(R_{\alpha\beta}, R_{\alpha\gamma}, R_{\beta\gamma}, R_{co}) \tag{54}$$

where E^{in}_{sc} represents an explicit function of the four variables $R_{\alpha\beta}$, $R_{\alpha\gamma}$, $R_{\beta\gamma}$, and R_{co}. Likewise, the shape functional

$$\mathcal{F}^{in}_{sc} \equiv \mathcal{F}^{in}\{S_{sc}\} = F^{in}_{sc}(R_{\alpha\beta}, R_{\alpha\gamma}, R_{\beta\gamma}, R_{co}) \tag{55}$$

also becomes an explicit function of the four radii. Constrained energy minimization within the subspace of three-spherical-cap shapes then implies the four stationarity relations

$$\frac{\partial F^{in}_{sc}}{\partial R_{\alpha\beta}} = 0, \quad \frac{\partial F^{in}_{sc}}{\partial R_{\alpha\gamma}} = 0, \quad \frac{\partial F^{in}_{sc}}{\partial R_{\beta\gamma}} = 0, \quad \text{and} \quad \frac{\partial F^{in}_{sc}}{\partial R_{co}} = 0 \tag{56}$$

It is not difficult to show that the first condition $\frac{\partial F^{in}_{sc}}{\partial R_{\alpha\beta}} = 0$ is equivalent to the classical Laplace equation (25) for the curvature radius $R_{\alpha\beta}$ of the $\alpha\beta$ interface. We should also require that the two stationarity relations $\frac{\partial F^{in}_{sc}}{\partial R_{\alpha\gamma}} = 0$ and $\frac{\partial F^{in}_{sc}}{\partial R_{\beta\gamma}} = 0$ lead back to the shape equations (32) for the curvature radii $R_{\alpha\gamma}$ and $R_{\beta\gamma}$ of the two membrane segments. The latter requirement is, however, not fulfilled in general but only for certain regions of the parameter space corresponding to small and large spontaneous curvatures. In these parameter regions, we can neglect those contributions to the bending energy (1) that involve the integrals over the mean curvature and over the mean curvature squared and focus on the remaining contributions to the energy functional $\mathcal{E}^{in}\{S_{sc}\}$ that depend on the four radii only via the three surface areas $A_{\alpha\beta}$, $A_{\alpha\gamma}$, and $A_{\beta\gamma}$.

Small Spontaneous Curvatures of Membrane Segments. The membrane segment $j\gamma$ of the three-spherical-cap shape S_{sc} has the bending energy

$$E^{in}_{j\gamma}\{S_{sc}\} \equiv 2\kappa_{j\gamma}A_{j\gamma}\left(\frac{1}{R_{j\gamma}} - m_{j\gamma}\right)^2 \tag{57}$$

The regime of small spontaneous curvature $m_{j\gamma}$ is now defined by

$$-\frac{1}{2R_{j\gamma}} \le m_{j\gamma} \le \frac{5}{2R_{j\gamma}} \qquad \text{(regime of small } m_{j\gamma}\text{)} \tag{58}$$

Because $A_{j\gamma} = 4\pi R_{j\gamma}{}^2\zeta_{j\gamma}$ with a dimensionless coefficient $\zeta_{j\gamma}$ that satisfies $0 < \zeta_{j\gamma} < 1$, the bending energy (57) of the $j\gamma$ segment can then be bounded from above by

$$E^{in}_{j\gamma} \le 18\pi\zeta_{j\gamma}\kappa_{j\gamma} \qquad \text{(regime of small } m_{j\gamma}\text{)} \tag{59}$$

Therefore, the contribution of the bending energy $E^{in}_{j\gamma}$ to the energy functional can be neglected compared to the contribution of the water−water interface if

$$E^{in}_{j\gamma} \le 18\pi\zeta_{j\gamma}\kappa_{j\gamma} \ll \Sigma_{\alpha\beta}A_{\alpha\beta} \tag{60}$$

which is fulfilled for

$$A_{\alpha\beta} \gg 18\pi\kappa_{j\gamma}/\Sigma_{\alpha\beta} \tag{61}$$

The bending rigidity $\kappa_{j\gamma}$ has the typical value $\kappa_{j\gamma} \simeq 10^{-19}$ J, whereas the observed values of the interfacial tension $\Sigma_{\alpha\beta}$ vary between 10^{-7} and 10^{-4} N/m. As a consequence, the bending energy of the membrane segment $j\gamma$ can be neglected compared to the free energy of the liquid−liquid interface if the spontaneous curvature is sufficiently small as in (58) and if the interfacial area $A_{\alpha\beta}$ is sufficiently large and satisfies $A_{\alpha\beta} \gg (7.5\ \mu\text{m})^2$ for $\Sigma_{\alpha\beta} = 10^{-7}$ N/m and $A_{\alpha\beta} \gg (0.24\ \mu\text{m})^2$ for $\Sigma_{\alpha\beta} = 10^{-4}$ N/m.

If the bending energies $E^{in}_{\alpha\gamma}\{S_{sc}\}$ and $E^{in}_{\beta\gamma}\{S_{sc}\}$ of both membrane segments can be neglected compared to the interfacial free energy, the stationarity relations (56) lead to the tension−angle relationships

$$\frac{\Sigma + W_{\alpha\gamma}}{\Sigma_{\alpha\beta}} = \frac{\sin\theta^{ap}_{\beta}}{\sin\theta^{ap}_{\gamma}} \quad \text{and} \quad \frac{\Sigma + W_{\beta\gamma}}{\Sigma_{\alpha\beta}} = \frac{\sin\theta^{ap}_{\alpha}}{\sin\theta^{ap}_{\gamma}} \tag{62}$$

which describes the force balance along the apparent contact line. This force balance can be visualized as a triangle, the sides of which are formed by the three tensions $\Sigma_{\alpha\beta}$, $\Sigma + W_{\alpha\gamma}$, and $\Sigma + W_{\beta\gamma}$, in close analogy to Neumann's triangle corresponding to the relationships (39) for the α and β droplets in the absence of the vesicle membrane.

Large Spontaneous Curvatures of Both Membrane Segments. The bending energy $E^{in}_{j\gamma}$ of the membrane segment $j\gamma$ becomes asymptotically equal to

$$E^{in}_{j\gamma}\{S_{sc}\} \approx \sigma_{j\gamma}A_{j\gamma} \quad \text{for large } |m_{j\gamma}| \gg M_{j\gamma} \tag{63}$$

with the spontaneous tension $\sigma_{j\gamma} = 2\kappa_{j\gamma}m_{j\gamma}{}^2$. If the bending energies of both membrane segments can be estimated by the expression (63), the stationarity conditions (56) lead to the generalized tension−angle relationships

$$\frac{\Sigma + W_{\alpha\gamma} + \sigma_{\alpha\gamma}}{\Sigma_{\alpha\beta}} = \frac{\sin\theta^{ap}_{\beta}}{\sin\theta^{ap}_{\gamma}} \quad \text{and} \quad \frac{\Sigma + W_{\beta\gamma} + \sigma_{\beta\gamma}}{\Sigma_{\alpha\beta}} = \frac{\sin\theta^{ap}_{\alpha}}{\sin\theta^{ap}_{\gamma}} \tag{64}$$

which again describes the force balance along the apparent contact line. Now, this force balance corresponds to a triangle that is formed by the three tensions $\Sigma_{\alpha\beta}$, $\Sigma + W_{\alpha\gamma} + \sigma_{\alpha\gamma}$, and $\Sigma + W_{\beta\gamma} + \sigma_{\beta\gamma}$.

One Large and One Small Spontaneous Curvature. Another special parameter region is obtained if one spontaneous curvature is large whereas the other one is small. If $m_{\alpha\gamma}$ is large, the bending energy of the $\alpha\gamma$ membrane segment can be estimated by the relation (63) with $j = \alpha$. Furthermore, if $m_{\beta\gamma}$ is small and satisfies the inequalities (58) with $j = \beta$, the bending energy of the $\beta\gamma$ segment can be neglected for a sufficiently large area $A_{\alpha\beta}$ of the $\alpha\beta$ interface as described by (61) with $j = \beta$. For this parameter regime, we obtain the tension−angle relationships

$$\frac{\Sigma + W_{\alpha\gamma} + \sigma_{\alpha\gamma}}{\Sigma_{\alpha\beta}} = \frac{\sin\theta^{ap}_{\beta}}{\sin\theta^{ap}_{\gamma}} \quad \text{and} \quad \frac{\Sigma + W_{\beta\gamma}}{\Sigma_{\alpha\beta}} = \frac{\sin\theta^{ap}_{\alpha}}{\sin\theta^{ap}_{\gamma}} \tag{65}$$

Formation of Membrane Nanotubes. A GUV membrane with a large spontaneous curvature and, thus, a large spontaneous tension can relax this tension by forming membrane nanotubes.[28] Therefore, if one of the membrane segments

DOI: 10.1021/acs.jpcb.7b10783
J. Phys. Chem. B 2018, 122, 3572−3586

acquires a large spontaneous curvature because of wetting, this segment has a tendency to form nanotubes. Such a tubulation process has indeed been observed during the deflation of GUVs that contained aqueous PEG−dextran solutions.[25,26] Both experiments and simulations provide strong evidence that the PEG molecules are adsorbed onto the GUV membranes. When the two leaflets of the bilayer membranes are exposed to different PEG concentrations, the two adsorption layers are asymmetric and can generate large spontaneous curvatures and large spontaneous tensions.

The phase diagram of aqueous PEG−dextran solutions is schematically depicted in Figure 5. This phase diagram exhibits

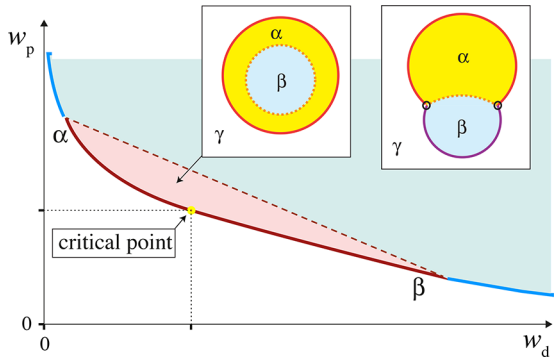

Figure 5. Schematic phase diagram of aqueous PEG−dextran solutions as a function of the weight fractions w_d and w_r for dextran and PEG, experimentally determined in ref 26. The coexistence region of the PEG-rich phase α and the dextran-rich phase β contains two subregions, a complete wetting (pink) and a partial wetting (turquois) region. In the pink subregion close to the critical point, the membrane is completely wetted by the PEG-rich phase α which encloses the dextran-rich phase β; see left inset. In the turquoise subregion, the membrane is partially wetted by both phases; see right inset. The boundary between the complete and partial subregions is provided by a certain tie line (dashed straight line), the precise location of which depends on the lipid composition of the membrane. Along this tie line, the system undergoes a complete-to-partial wetting transition. The $\alpha\gamma$ membrane segments are observed to form membrane nanotubes (not shown) that stay away from the $\alpha\beta$ interface for complete wetting but adhere to this interface for partial wetting.

a two-phase coexistence region with both a complete wetting regime close to the critical point and a partial wetting regime further away from this point. The two wetting regimes are separated by a certain tie line, as indicated by the dashed straight line in Figure 5. In the complete wetting regime, the whole vesicle membrane is in contact with the PEG-rich phase α and forms nanotubes. In contrast, in the partial wetting regime, only the $\alpha\gamma$ membrane segment in contact with the PEG-rich phase formed such tubes. Furthermore, for complete wetting, the tubes stayed away from the $\alpha\beta$ interface, whereas they accumulated on this interface for partial wetting. In the latter case, the adhesion of the tubes to the $\alpha\beta$ interface lowers the (free) energy of the vesicle−droplet system, as explicitly shown in ref 26. Each tube that adheres to the $\alpha\beta$ interface is in contact with both the α and the β phase and, thus, forms both an $\alpha\gamma$ and a $\beta\gamma$ membrane segment separated by a contact line parallel to the long tube axis. Along these microscopic contact lines, the angle between the $\alpha\beta$ interface and the $\alpha\gamma$ tube segments is again given by the intrinsic contact angle θ_α^* with the same local geometry as depicted in Figure 2b, where γ now represents the liquid phase within the tubes.

If the $\alpha\gamma$ membrane segment forms nanotubes, the segment tension $\Sigma_{\alpha\gamma} = \Sigma + W_{\alpha\gamma}$ is small compared to the spontaneous tension $\sigma_{\alpha\gamma}$ of this segment as follows from the mechanical equilibrium between the highly curved tubes and the weakly curved spherical $\alpha\gamma$ segments.[28] The corresponding tension−angle relationship in (64) and (65) then assumes the simplified form

$$\frac{\sigma_{\alpha\gamma}}{\Sigma_{\alpha\beta}} = \frac{2\kappa_{\alpha\gamma} m_{\alpha\gamma}^{\ 2}}{\Sigma_{\alpha\beta}} \approx \frac{\sin\theta_\beta^{\mathrm{ap}}}{\sin\theta_\gamma^{\mathrm{ap}}} \qquad \text{(tubulated } \alpha\gamma \text{ segments)} \tag{66}$$

which can be used to estimate the spontaneous curvature $m_{\alpha\gamma}$ from the apparent contact angles.[26]

TWO-DROPLET VESICLES WITH CLOSED NECKS

For partial in-wetting, the vesicle membrane is in contact with two enclosed droplets, as displayed in Figure 3a,b. When we deflate such a two-droplet vesicle, it can decrease its interfacial energy by reducing the area of the $\alpha\beta$ interface. The corresponding energy gain is $\Delta A_{\alpha\beta}\Sigma_{\alpha\beta}$, where $\Delta A_{\alpha\beta}$ is the change in the interfacial area. Such a morphological change is, in fact, rather likely unless one of the membrane segments has a sufficiently large spontaneous curvature to form nanobuds and nanotubes. Thus, let us assume that the $\alpha\gamma$ segment forms such protrusions. The corresponding energy gain is $\Delta A_{\alpha\gamma}\sigma_{\alpha\gamma}$ with the area $\Delta A_{\alpha\gamma}$ stored in the nanotubes and the spontaneous tension $\sigma_{\alpha\gamma} = 2\kappa_{\alpha\gamma} m_{\alpha\gamma}^{\ 2}$. Therefore, the osmotic deflation of a partially wetted vesicle should reduce the area of the $\alpha\beta$ interface whenever $\Delta A_{\alpha\beta}\Sigma_{\alpha\beta} \gg \Delta A_{\alpha\gamma}\sigma_{\alpha\gamma}$ which is typically fulfilled for $\Sigma_{\alpha\beta} \gg \sigma_{\alpha\gamma}$.

In the absence of nanobud or nanotube formation, the area of the $\alpha\beta$ interface will eventually shrink to zero and the vesicle membrane will then form a closed membrane neck around this point-like interface, as depicted in Figure 1d. This special in-wetting morphology, which resembles complete wetting by the γ phase, is only possible if the vesicle membrane can enclose both liquid droplets which implies that the membrane area A must satisfy the inequality

$$A \geq A_{2\mathrm{sp}} = (4\pi)^{1/3}(3V_\alpha)^{2/3} + (4\pi)^{1/3}(3V_\beta)^{2/3} \tag{67}$$

with the volumes V_α and V_β of the two spherical droplets.

Two-sphere shapes with closed membrane necks can also be formed by two-domain vesicles arising from lipid phase separation within multicomponent membranes.[31] Compared to such two-domain vesicles, the closed neck of a two-droplet vesicle is further stabilized by the formation of the $\alpha\beta$ interface during neck opening. If we ignore the possible difference of the Gaussian curvature moduli $\kappa_{G,\alpha\gamma}$ and $\kappa_{G,\beta\gamma}$, the contact line is located within the membrane neck and the contact line radius r_1 is equal to the neck radius R_{ne}. The free energy of the membrane neck then includes a contribution from the neck-spanning $\alpha\beta$ interface which has the form

$$\Sigma_{\alpha\beta}A_{\alpha\beta} = \frac{2\pi}{1 + \sin\theta_\alpha^*}\Sigma_{\alpha\beta}R_{\mathrm{ne}}^{\ 2} \tag{68}$$

which depends on the intrinsic contact angle θ_α^*, see Figure 2b, and grows quadratically with increasing neck radius R_{ne}. The bending energy of the vesicle membrane that consists of two membrane segments and forms an open neck of radius R_{ne} can be obtained from the corresponding expression for two-domain vesicles as derived in ref 31. Adding the free energy of the contact line, we then obtain

$$E_{\mathrm{be}}(R_{\mathrm{ne}}) + 2\pi R_{\mathrm{ne}}\lambda_{\mathrm{co}} \approx E_{\mathrm{be}}(R_{\mathrm{ne}} = 0) - 4\pi E_1 R_{\mathrm{ne}} \qquad \text{for small } R_{\mathrm{ne}} \tag{69}$$

DOI: 10.1021/acs.jpcb.7b10783
J. Phys. Chem. B 2018, 122, 3572−3586

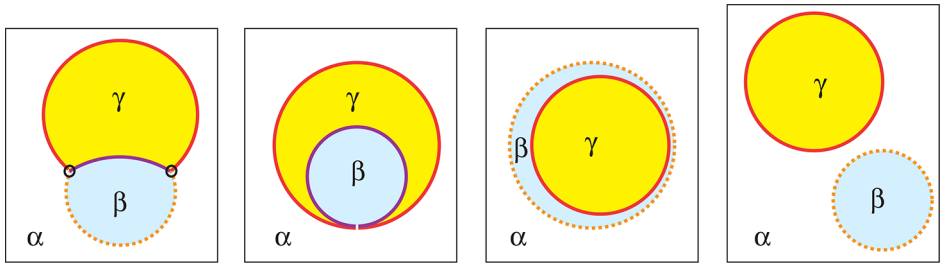

Figure 6. Out-wetting morphologies arising from phase separation into two aqueous phases, α (white) and β (blue), *outside* a giant vesicle which is filled with the aqueous spectator phase γ. The β phase forms a droplet or layer that coexists with the bulk liquid α: (a) Partial wetting of the vesicle membrane by α and β as observed on the micrometer scale. The apparent kink at the contact line (black circles) again reveals the capillary forces that the $\alpha\beta$ interface exerts onto the vesicle membfane. (b) Special morphology for which the β droplet and the bulk phase α are separated by a closed membrane neck. This morphology, which resembles complete wetting by the γ phase, is only possible if the membrane has a certain minimal area. (c) Complete wetting of the membrane by the β phase. (d) Complete wetting by the α phase. The color code for the two membrane segments and the $\alpha\beta$ interface is the same as that in Figure 1.

with

$$E_1 \equiv \kappa_{\alpha\gamma}(M_{\alpha\gamma} - m_{\alpha\gamma}) + \kappa_{\beta\gamma}(M_{\beta\gamma} - m_{\beta\gamma}) - \frac{1}{2}\lambda_{co} \tag{70}$$

The closure of the neck and the stability of the closed neck are governed by the behavior of the combined free energy $\Sigma_{\alpha\beta}A_{\alpha\beta} + E_{be}(R_{ne}) + 2\pi R_{ne}\lambda_{co}$ for small R_{ne}. In the latter limit, the leading term is provided by the E_1-term in (69) because the interfacial free energy is $\Sigma_{\alpha\beta}A_{\alpha\beta} \sim R_{ne}^2$. Therefore, we obtain the stability criterion $E_1 \leq 0$ which is equivalent to

$$\kappa_{\beta\gamma}(M_{\beta\gamma} - m_{\beta\gamma}) + \kappa_{\alpha\gamma}(M_{\alpha\gamma} - m_{\alpha\gamma}) \leq \frac{1}{2}\lambda_{co} \qquad (\kappa_{G,\beta\gamma} \simeq \kappa_{G,\alpha\gamma}) \tag{71}$$

The equality in eq 71 describes the neck closure condition for the limit shapes as obtained from vesicle shapes with open necks, whereas the inequality describes the stability of closed necks.

OUT-WETTING MORPHOLOGIES

So far, we have discussed in-wetting morphologies of GUVs that arise from aqueous phase separation within the vesicles. As mentioned in the Introduction, wetting of vesicle membranes has also been observed when the PEG–dextran solutions underwent phase separation outside the GUVs.[27] The aqueous minority phase then forms droplets that can adhere to the vesicle membrane. The adhesion of one such droplet leads to several out-wetting morphologies, as shown in Figure 6. The morphologies in Figure 6a and b have been observed for PEG–dextran solutions.[27] The morphology in Figure 6a corresponds to partial wetting of the vesicle membrane by both α and β. This morphology is again characterized by a three-phase contact line that partitions the membrane into two segments. When viewed with optical resolution, the shape contour had again an apparent kink close to the contact line which should be replaced by a smoothly curved membrane segment when we look at this line with nanoscale resolution.

For partial out-wetting, the $\alpha\beta$ interface partitions the vesicle membrane into an $\gamma\alpha$ segment and a $\gamma\beta$ segment. At first sight, swapping the subscripts γ and α as well as γ and β for out-wetting compared to in-wetting morphologies might seem a bit pedantic but turns out to be important because of the spontaneous curvatures. These curvatures have a sign that is taken to be positive and negative if the membrane prefers to bulge toward the exterior and interior solution, respectively. Therefore, when we swap the interior and exterior solutions, the spontaneous curvature $m_{\gamma j}$ for out-wetting morphologies differs from the spontaneous curvature $m_{i\gamma} = -m_{\gamma j}$ for in-wetting morphologies.

The theory for out-wetting can be developed in close analogy to the theory for in-wetting as described above. Thus, we define the three mean curvatures $M_{\gamma\alpha} = 1/R_{\gamma\alpha} > 0$, $M_{\gamma\beta} = \pm 1/R_{\beta\gamma}$, and $M_{\alpha\beta} = 1/R_{\alpha\beta} > 0$ of the three spherical surface segments in Figure 6a. Note that $M_{\gamma\beta}$ is positive if $P_\gamma > P_\beta$ and negative otherwise. Likewise, we introduce three apparent contact angles θ_γ^{ap}, θ_β^{ap}, and θ_α^{ap} that open up toward the three liquid phases γ, β, and α as well as the effective tensions

$$\Sigma_{\gamma j}^{eff} \equiv \Sigma + W_{\gamma j} + \sigma_{\gamma j} - 2\kappa_{\gamma j} m_{\gamma j} M_{\gamma j} \tag{72}$$

with $j = \alpha, \beta$. The tension–angle–curvature relationship for partial out-wetting is then given by

$$M_{\gamma\alpha}\left(\frac{\Sigma_{\gamma\alpha}^{eff}}{\Sigma_{\alpha\beta}} - \frac{\sin\theta_\beta^{ap}}{\sin\theta_\gamma^{ap}}\right) = M_{\gamma\beta}\left(\frac{\Sigma_{\gamma\beta}^{eff}}{\Sigma_{\alpha\beta}} - \frac{\sin\theta_\alpha^{ap}}{\sin\theta_\gamma^{ap}}\right) \tag{73}$$

In contrast to in-wetting, the mean curvature $M_{\gamma\beta}$ of the $\gamma\beta$ membrane segment can now be negative corresponding to a $\gamma\beta$ segment that bulges toward the γ phase within the vesicle. When we apply the relationship (73) to GUVs for which the two mean curvatures $M_{\gamma\alpha}$ and $M_{\gamma\beta}$ fulfill certain relationships, see the in-wetting relationships (41)–(44), we can again obtain estimates for the material parameters of the vesicle–droplet system. Furthermore, when we consider special parameter regimes corresponding to small and large spontaneous curvatures $m_{\gamma j}$ as defined in analogy to (58) and (63), we again obtain tension–angle relationships for the force balance along the apparent contact lines.

In order to avoid any assumptions about the magnitude of the overall stress Σ, we can now consider several β droplets adhering to the exterior leaflet of the same GUV membrane. We then obtain several $\gamma\beta$ segments which we distinguish by the label $n = 1, 2, \ldots, N$. These $\gamma\beta$ segments have the mean curvatures $M_{\gamma\beta}^{(n)}$ and experience the effective tensions $\Sigma_{\gamma\beta}^{(n)}$. We then obtain the relations $\Upsilon_{\gamma\beta}^{(1)} = \Upsilon_{\gamma\beta}^{(2)} = \cdots = \Upsilon_{\gamma\beta}^{(N)}$ with

$$\Upsilon_{\gamma\beta}^{(n)} \equiv M_{\gamma\alpha}\frac{\sin\theta_\beta^{(n)}}{\sin\theta_\gamma^{(n)}} + M_{\gamma\beta}^{(n)}\left(\frac{\Sigma_{\gamma\beta}^{(n)}}{\Sigma_{\alpha\beta}} - \frac{\sin\theta_\alpha^{(n)}}{\sin\theta_\gamma^{(n)}}\right) \tag{74}$$

in close analogy to the relations (52) and (53) for in-wetting. Thus, from three different $\gamma\beta$ segments with three distinct mean curvatures $M_{\gamma\beta}^{(n)}$, we can obtain the two parameter combinations $(\Sigma + W_{\gamma\beta} + \sigma_{\gamma\beta})/\Sigma_{\alpha\beta}$ and $\kappa_{\gamma\beta}m_{\gamma\beta}/\Sigma_{\alpha\beta}$ that determine the tension ratios $\Sigma_{\gamma\beta}^{(n)}/\Sigma_{\alpha\beta}$.

DOI: 10.1021/acs.jpcb.7b10783
J. Phys. Chem. B 2018, 122, 3572–3586

CONCLUSIONS AND PERSPECTIVES

Partial wetting morphologies of giant vesicles exposed to aqueous two-phase systems as depicted in Figure 1a and Figure 6a for in- and out-wetting, respectively, are characterized by a three-phase contact line that partitions the vesicle membrane into two segments, an $\alpha\gamma$ or $\gamma\alpha$ segment in contact with the aqueous α phase, and a $\beta\gamma$ or $\gamma\beta$ segment in contact with the aqueous β phase. In contrast to previous theoretical studies, the theory presented here includes both the adhesion free energies of the two droplets and the overall lateral stress within the vesicle membrane.

The curvature elasticity of the vesicle membrane implies that, on the nanometer scale, this membrane bends smoothly along the contact line and then defines an intrinsic contact angle, as depicted in Figure 2 for partial in-wetting. This angle is related to the difference of the segment tensions as given by the force balance eq 17. The latter equation also depends on the local curvatures of the two membrane segments at the contact line. At present, these curvatures cannot be determined experimentally, which implies that the relations (17)−(19) cannot be used to analyze experimental observations. However, the experiments revealed that the two membrane segments form spherical caps which define an apparent contact line and apparent contact angles as displayed in Figure 3 for partial in-wetting. The spherical cap geometry leads to the simplified shape equations (31) which imply the general relationship (37) for partial in-wetting. The latter relationship depends on the effective tensions and curvature radii of the two membrane segments as well as on the apparent contact angles. This relationship, which is reminiscent of Neumann's triangle but depends on the droplet radii $R_{\alpha\gamma} = 1/M_{\alpha\gamma}$ and $R_{\beta\gamma} = 1/M_{\beta\gamma}$, can be used to deduce the material parameters of the vesicle−droplet system from the observed wetting morphology. Vesicles with several adhering droplets lead to the relationships (52) and (53) by which we can deduce certain parameter combinations without making any assumptions about the overall lateral stress Σ or about the mean curvatures of the membrane segments. The analogous relationships for partial out-wetting are given by eq 73 and eq 74.

For certain regions of the parameter space corresponding to small and large spontaneous curvatures, another set of tension−angle relationships can be derived which describe the force balance along the apparent contact lines. For small spontaneous curvatures as defined by (58), the bending energies can be neglected compared to the interfacial free energy of the $\alpha\beta$ interface provided the interfacial area $A_{\alpha\beta}$ is sufficiently large and satisfies the inequality (61). In this parameter regime, we obtain the tension−angle relationships (62). For large spontaneous curvatures for which the bending energy is dominated by the spontaneous tension and behaves as in (63), the force balance is given by the generalized tension−angle relationships (64). If one of the membrane segments forms membrane nanotubes, the corresponding tension−angle relationship simplifies and one can use the resulting relationship (66) to estimate the spontaneous curvature of the tubulated segment.

The material parameters determined from the different relationships derived above remain unchanged when we move along a tie line within the phase diagram of the aqueous two-phase system; compare Figure 5. Thus, it would be particularly useful to experimentally study several two-phase systems that belong to the same tie line, including the two end points of this line. At these end points, the GUVs are completely filled with one of the two coexisting phases and the GUV membranes consist of a single segment. The material properties of these single membrane segments must be identical with the corresponding properties of the membrane segments that govern the partial wetting morphologies along the whole tie line between the two end points.

In the present study, we have largely ignored the line tension λ_{co} of the contact line which is justified if the contact line radius is sufficiently large as implied by the force balance relation (17). One exception is two-droplet vesicles with closed necks for which the contact line radius vanishes. The stability of this neck is described by (71) which depends explicitly on the line tension λ_{co}. The latter tension will also play an important role for nucleation and growth of aqueous nanodroplets at membranes. In contrast to the line tension of domain boundaries which must be positive to ensure the stability of the domains, the line tension of the contact line can be positive or negative. This aspect can be studied by molecular dynamics simulations as will be described elsewhere.

One open problem that could be addressed by numerical studies of the shape equations is the dependence of the intrinsic contact angle on the vesicle geometry. For zero spontaneous curvatures and large contact line radius, the intrinsic contact angle depends only on the adhesive strengths of the two droplets and on the interfacial tension of the water−water interface, see the force balance equation (20), which implies that the intrinsic contact angle is a material parameter as one might expect intuitively. However, for two membrane segments with different curvature-elastic properties, the intrinsic contact angle also depends on the local membrane curvatures at the contact line, see the relations (17)−(19), and these curvatures are expected to depend on the vesicle geometry.

Another aspect of vesicle−droplet morphologies that provides an interesting challenge for future studies is the possible interplay between aqueous phase separation leading to liquid droplets and membrane phase separation leading to intramembrane domains. From the theoretical point of view, this interplay leads to a variety of interesting cases. For example, each of the two aqueous phases α and β may prefer one of the two membrane phases, say a and b. In such a situation, the nucleation of α and β droplets will be facilitated on the a and b domains, respectively. Furthermore, once the aqueous phase separation has been completed into one large α droplet and one large β droplet, the a and b domains will try to maximize their contact area with the α and β droplets. It is certainly of interest to study these processes in a systematic manner, both by theory and by experiment.

Aqueous two-phase systems are frequently used in chemical analysis and biotechnology for the sorting and separation of cellular membranes, membrane-bound organelles, and cells.[1] During these processes, the different cellular membranes are exposed to two aqueous phases. Understanding the wetting properties of these systems is of some practical value. On the one hand, it may be desirable to ensure that the cellular membranes are always completely wetted by one of the aqueous phases. On the other hand, the response of partially wetted membranes to capillary forces could be used to elucidate the mechanical properties of organelles and cells as well.

A particularly interesting class of aqueous droplets is provided by membrane-less or droplet-like organelles that have been recently discovered *in vivo*[36] and are enriched in intrinsically disordered proteins[37] such as FUS. These droplet-like organelles can be reconstituted *in vitro* which leads to novel kinds of water-in-water emulsions. The interaction of the resulting water-in-water droplets with biomimetic and biological membranes

DOI: 10.1021/acs.jpcb.7b10783
J. Phys. Chem. B 2018, 122, 3572−3586

represents another intriguing topic for future research with direct implications for molecular cell biology.

AUTHOR INFORMATION

Corresponding Author

*E-mail: lipowsky@mpikg.mpg.de.

ORCID

Reinhard Lipowsky: 0000-0001-8417-8567

Notes

The author declares no competing financial interest.

ACKNOWLEDGMENTS

I thank Roland Knorr, Titus Franzmann, Anthony Hyman, and Rumiana Dimova as well as Vahid Satarifard and Andrea Grafmüller for fruitful collaborations on vesicle−droplet systems.

GLOSSARY WITH MATHEMATICAL SYMBOLS

A total membrane area, $A = A_{\alpha\gamma} + A_{\beta\gamma}$
$A_{\alpha\beta}$ surface area of the $\alpha\beta$ interface
$A_{\alpha\gamma}$ surface area of the $\alpha\gamma$ membrane segment.
$A_{\beta\gamma}$ surface area of the $\beta\gamma$ membrane segment
α, β two coexisting liquid phases, Figure 1
$\alpha\beta$ indicates the interface between the α and β phases
$\alpha\gamma$ indicates the membrane segment between the α and γ phases
$\beta\gamma$ indicates the membrane segment between the β and γ phases
C_1 principal curvature along the contour of an axisymmetric shape
C_2 principal curvature orthogonal to C_1
$E_{\mathrm{be}}^{\mathrm{in}}$ bending energy of membrane for in-wetting morphology
$E_{j\gamma}^{\mathrm{in}}$ bending energy of the $j\gamma$ membrane segment forming a spherical cap, eq 57
E_{G} Gaussian curvature energy
E_{ad} adhesion free energy of the vesicle−droplet system
$\mathcal{E}^{\mathrm{in}}$ energy functional of the vesicle−droplet system for in-wetting, eq 9
$\mathcal{F}^{\mathrm{in}}$ shape functional of the vesicle−droplet system for in-wetting, eq 10
G Gaussian curvature
γ liquid phase that plays the role of a spectator phase, Figure 1 and Figure 6
j index with $j = \alpha$ or $j = \beta$
K_A area compressibility modulus
$\kappa_{\alpha\gamma}$ bending rigidity of the $\alpha\gamma$ membrane segment
$\kappa_{\beta\gamma}$ bending rigidity of the $\beta\gamma$ membrane segment
$\kappa_{\mathrm{G},\alpha\gamma}$ Gaussian curvature modulus of the $\alpha\gamma$ membrane segment
$\kappa_{\mathrm{G},\beta\gamma}$ Gaussian curvature modulus of the $\beta\gamma$ membrane segment
L_{co} length of the contact line between the $\alpha\beta$ interface and the vesicle membrane
λ_{co} line tension of contact line
$m_{\alpha\gamma}$ spontaneous curvature of the $\alpha\gamma$ membrane segment
$m_{\beta\gamma}$ spontaneous curvature of the $\beta\gamma$ membrane segment
M mean curvature
$M_{\alpha\beta}$ mean curvature of the $\alpha\beta$ interface
$M_{\alpha\gamma}$ mean curvature of the $\alpha\gamma$ membrane segment forming a spherical cap
$M_{\beta\gamma}$ mean curvature of the $\beta\gamma$ membrane segment forming a spherical cap
P_α pressure in the liquid phase α
P_β pressure in the liquid phase β
P_γ pressure in the liquid phase γ
ψ tilt angle used to parametrize axisymmetric vesicle shape, Figure 2
r radial coordinate for axisymmetric vesicle shape, Figure 2
r_1 radius of contact line, $r_1 = r(s_1)$
$R_{\alpha\beta}$ curvature radius of the $\alpha\beta$ interface, Figure 3
$R_{\alpha\gamma}$ curvature radius of the $\alpha\gamma$ membrane segment forming a spherical cap, Figure 3
$R_{\beta\gamma}$ curvature radius of the $\beta\gamma$ membrane segment forming a spherical cap, Figure 3
R_{co} radius of the contact line, Figure 3
R_{ne} radius of the membrane neck
s arc length of the contour of an axisymmetric vesicle
s_1 arc length value for the contact line position
S shape of the vesicle−droplet system
S_{sc} three-spherical-cap shape of the vesicle−droplet system
$\sigma_{\alpha\gamma}$ spontaneous tension of the $\alpha\gamma$ membrane segment, $\sigma_{\alpha\gamma} = 2\kappa_{\alpha\gamma}m_{\alpha\gamma}^2$
$\sigma_{\beta\gamma}$ spontaneous tension of the $\beta\gamma$ membrane segment, $\sigma_{\beta\gamma} = 2\kappa_{\beta\gamma}m_{\beta\gamma}^2$
Σ overall lateral stress within the vesicle membrane
$\Sigma_{\alpha\beta}$ interfacial tension of the $\alpha\beta$ interface
$\Sigma_{\alpha\gamma}$ mechanical tension of the $\alpha\gamma$ membrane segment, $\Sigma_{\alpha\gamma} = \Sigma + W_{\alpha\gamma}$, in-wetting
$\Sigma_{\beta\gamma}$ mechanical tension of the $\beta\gamma$ membrane segment, $\Sigma_{\beta\gamma} = \Sigma + W_{\beta\gamma}$, in-wetting
$\Sigma_{j\gamma}^{\mathrm{eff}}$ effective tension of the $j\gamma$ membrane segment for in-wetting, eq 35
$\Sigma_{\alpha\gamma}^{(n)}$ effective tension $\Sigma_{\alpha\gamma}^{\mathrm{eff}}$ of the $\alpha\gamma$ segment with number n, in-wetting
$\Sigma_{\gamma\alpha}$ mechanical tension of the $\gamma\alpha$ membrane segment, $\Sigma_{\gamma\alpha} = \Sigma + W_{\gamma\alpha}$, out-wetting
$\Sigma_{\gamma\beta}$ mechanical tension of the $\gamma\beta$ membrane segment, $\Sigma_{\gamma\beta} = \Sigma + W_{\gamma\beta}$, out-wetting
$\Sigma_{\gamma j}^{\mathrm{eff}}$ effective tension of the γj membrane segment for out-wetting, eq 72
$\Sigma_{\gamma\beta}^{(n)}$ effective tension $\Sigma_{\gamma\beta}^{\mathrm{eff}}$ of the $\gamma\beta$ segment with number n, out-wetting
θ contact angle
θ_α^* intrinsic contact angle between the $\alpha\beta$ interface and the $\alpha\gamma$ membrane segment
θ_β^* intrinsic contact angle with $\theta_\beta^* = \pi - \theta_\alpha^*$
$\theta_\alpha^{\mathrm{ap}}$ apparent contact angle that opens up toward the α phase
$\theta_\beta^{\mathrm{ap}}$ apparent contact angle that opens up toward the β phase
$\theta_\gamma^{\mathrm{ap}}$ apparent contact angle that opens up toward the γ phase, $\theta_\gamma^{\mathrm{ap}} = 2\pi - \theta_\alpha^{\mathrm{ap}} - \theta_\beta^{\mathrm{ap}}$
$\theta_\alpha^{(n)}$ apparent contact angle $\theta_\alpha^{\mathrm{ap}}$ for droplet number n
$\theta_\beta^{(n)}$ apparent contact angle $\theta_\beta^{\mathrm{ap}}$ for droplet number n
$\theta_\gamma^{(n)}$ apparent contact angle $\theta_\gamma^{\mathrm{ap}}$ for droplet number n
V_α volume of α droplet
V_β volume of β droplet
W adhesion energy per unit area or adhesive strength
$W_{\alpha\gamma}$ adhesive strength between membrane and α droplet
$W_{\beta\gamma}$ adhesive strength between membrane and β droplet
z Cartesian coordinate and axis of rotational symmetry, Figure 2

REFERENCES

(1) Albertsson, P. A. *Partition of Cell Particles and Macromolecules*, 3rd ed.; Wiley: 1986.

(2) Esquena, J. Water-in-Water (W/W) Emulsions. *Curr. Opin. Colloid Interface Sci.* **2016**, *25*, 109−119.

DOI: 10.1021/acs.jpcb.7b10783
J. Phys. Chem. B 2018, 122, 3572−3586

(3) Freire, M. G.; Cláudio, A. F. M.; Coutinho, J. A. P.; Marrucho, I. M.; Lopes, J. N. C.; Rebelo, L. P. N. Aqueous Biphasic Systems: a Boost Brought about by Using Ionic Liquids. *Chem. Soc. Rev.* **2012**, *41*, 4966−4995.
(4) Soares, R. R. G.; Azevedo, A. M.; Alstine, J. M. V.; Aires-Barros, M. R. Partitioning in Aqueous Two-Phase Systems: Analysis of Strengths, Weaknesses, Opportunities and Threats. *Biotechnol. J.* **2015**, *10*, 1158−1169.
(5) Grilo, A. L.; Aires-Barros, M. R.; Azevedo, A. M. Partitioning in Aqueous Two-Phase Systems: Fundamentals, Applications and Trends. *Sep. Purif. Rev.* **2016**, *45*, 68−80.
(6) Boreyko, J. B.; Mruetusatorn, P.; Retterer, S. T.; Collier, C. P. Aqueous Two-Phase Microdroplets with Reversible Phase Transitions. *Lab Chip* **2013**, *13*, 1295−1301.
(7) Balakrishnan, G.; Nicolai, T.; Benyahia, L.; Durand, D. Particle Trapped at the Droplet Interface in Water-in-Water Emulsions. *Langmuir* **2012**, *28*, 5921−5926.
(8) Vis, M.; Opdam, J.; van't Oor, I. S. J.; Soligno, G.; van Roij, R.; Tromp, R. H.; Erné, B. H. Water-in-Water Emulsions stabilized by Nanoplates. *ACS Macro Lett.* **2015**, *4*, 965−968.
(9) Xue, L.-H.; Xie, C.-Y.; Meng, S.-X.; Bai, R.-X.; Yang, X.; Wang, Y.; Wang, S.; Binks, B. P.; Guo, T.; Meng, T. Polymer²'Protein Conjugate Particles with Biocatalytic Activity for Stabilization at Water-in-Water Emulsions. *ACS Macro Lett.* **2017**, *6*, 679−683.
(10) Chatsisvili, N.; Philipse, A. P.; Loppinet, B.; Tromp, R. H. Colloidal Zein Particles at Water-Water interfaces. *Food Hydrocolloids* **2017**, *65*, 17−23.
(11) Scholten, E.; Tuinier, R.; Tromp, R. H.; Lekkerkerker, H. N. W. Interfacial Tension of a Decomposed Biopolymer Mixture. *Langmuir* **2002**, *18*, 2234−2238.
(12) Liu, Y.; Lipowsky, R.; Dimova, R. Concentration Dependence of the Interfacial Tension for Aqueous Two-Phase Polymer Solutions of Dextran and Polyethylene Glycol. *Langmuir* **2012**, *28*, 3831−3839.
(13) Atefi, E.; Mann, J. A.; Tavana, H. Ultralow Interfacial Tensions of Aqueous Two-Phase Systems Measured Using Drop Shape. *Langmuir* **2014**, *30*, 9691−9699.
(14) de Freitas, R. A.; Nicolai, T.; Chassenieux, C.; Benyahia, L. Stabilization of Water-in-Water Emulsions by Polysaccharide-Coated Protein Particles. *Langmuir* **2016**, *32*, 1227−1232.
(15) Rowlinson, J.; Widom, B. *Molecular Theory of Capillarity*; Clarendon Press: Oxford, U.K., 1989.
(16) Helfrich, W. Elastic Properties of Lipid Bilayers: Theory and Possible Experiments. *Z. Naturforsch., C: J. Biosci.* **1973**, *28c*, 693−703.
(17) Seifert, U.; Berndl, K.; Lipowsky, R. Shape Transformations of Vesicles: Phase Diagram for Spontaneous Curvature and Bilayer Coupling Model. *Phys. Rev. A: At., Mol., Opt. Phys.* **1991**, *44*, 1182−1202.
(18) Lipowsky, R., Sackmann, E., Eds. *Structure and Dynamics of Membranes: From Cells to Vesicles; Handbook of Biological Physics*; Elsevier: Amsterdam, The Netherlands, 1995; Vol. *1*.
(19) Dimova, R., Marques, C., Eds. *The Giant Vesicle Book*; Taylor & Francis: in press.
(20) Li, Y.; Lipowsky, R.; Dimova, R. Transition from Complete to Partial Wetting within Membrane Compartments. *J. Am. Chem. Soc.* **2008**, *130*, 12252−12253.
(21) Helfrich, M.; Mangeney-Slavin, L.; Long, M.; Djoko, K.; Keating, C. Aqueous Phase Separation in Giant Vesicles. *J. Am. Chem. Soc.* **2002**, *124*, 13374−13375.
(22) Long, M. S.; Jones, C. D.; Helfrich, M. R.; Mangeney-Slavin, L. K.; Keating, C. D. Dynamic Microcompartmentation in Synthetic Cells. *Proc. Natl. Acad. Sci. U. S. A.* **2005**, *102*, 5920−5925.
(23) Long, M. S.; Cans, A. S.; Keating, C. D. Budding and Asymmetric Protein Microcompartmentation in Giant Vesicles Containing Two Aqueous Phases. *J. Am. Chem. Soc.* **2008**, *130*, 756−762.
(24) Kusumaatmaja, H.; Li, Y.; Dimova, R.; Lipowsky, R. Intrinsic Contact Angle of Aqueous Phases at Membranes and Vesicles. *Phys. Rev. Lett.* **2009**, *103*, 238103.
(25) Li, Y.; Lipowsky, R.; Dimova, R. Membrane Nanotubes Induced by Aqueous phase Separation and Stabilized by Spontaneous Curvature. *Proc. Natl. Acad. Sci. U. S. A.* **2011**, *108*, 4731−4736.
(26) Liu, Y.; Agudo-Canalejo, J.; Grafmüller, A.; Dimova, R.; Lipowsky, R. Patterns of Flexible Nanotubes Formed by Liquid-Ordered and Liquid-Disordered Membranes. *ACS Nano* **2016**, *10*, 463−474.
(27) Li, Y.; Kusumaatmaja, H.; Lipowsky, R.; Dimova, R. Wetting-Induced Budding of Vesicles in Contact with Several Aqueous Phases. *J. Phys. Chem. B* **2012**, *116*, 1819−1823.
(28) Lipowsky, R. Spontaneous Tubulation of Membranes and Vesicles Reveals Membrane Tension Generated by Spontaneous Curvature. *Faraday Discuss.* **2013**, *161*, 305−331.
(29) Rawicz, W.; Olbrich, K. C.; McIntosh, T.; Needham, D.; Evans, E. Effect of Chain Length and Unsaturation on Elasticity of Lipid Bilayers. *Biophys. J.* **2000**, *79*, 328−339.
(30) do Carmo, M. *Differential Geometry of Curves and Surfaces*; Prentice-Hall: Englewood Cliffs, NJ, 1976.
(31) Jülicher, F.; Lipowsky, R. Shape Transformations of Inhomogeneous Vesicles with Intramembrane Domains. *Phys. Rev. E: Stat. Phys., Plasmas, Fluids, Relat. Interdiscip. Top.* **1996**, *53*, 2670−2683.
(32) Miao, L.; Seifert, U.; Wortis, M.; Döbereiner, H.-G. Budding Transitions of Fluid−Bilayer Vesicles: the Effect of Area−Difference Elasticity. *Phys. Rev. E: Stat. Phys., Plasmas, Fluids, Relat. Interdiscip. Top.* **1994**, *49*, 5389−5407.
(33) Döbereiner, H.-G.; Evans, E.; Kraus, M.; Seifert, U.; Wortis, M. Mapping Vesicle Shapes into the Phase Diagram: A Comparison of Experiment and Theory. *Phys. Rev. E: Stat. Phys., Plasmas, Fluids, Relat. Interdiscip. Top.* **1997**, *55*, 4458−4474.
(34) Lipowsky, R. Coupling of Bending and Stretching Deformations in Vesicle Membranes. *Adv. Colloid Interface Sci.* **2014**, *208*, 14−24.
(35) Zhong-can, O.-Y.; Helfrich, W. Bending Energy of Vesicle Membranes: General Expressions for the First, Second and Third Variation of the Shape Energy and Applications to Spheres and Cylinders. *Phys. Rev. A: At., Mol., Opt. Phys.* **1989**, *39*, 5280−5288.
(36) Brangwynne, C. P.; Eckmann, C. R.; Courson, D. S.; Rybarska, A.; Hoege, C.; Gharakhani, J.; Jülicher, F.; Hyman, A. A. Germline P Granules Are Liquid Droplets That Localize by Controlled Dissolution/Condensation. *Science* **2009**, *324*, 1729−1732.
(37) Bergeron-Sandoval, L.-P.; Safaee, N.; Michnick, S. W. Mechanisms and Consequences of Macromolecular Phase Separation. *Cell* **2016**, *165*, 1067−1079.

DOI: 10.1021/acs.jpcb.7b10783
J. Phys. Chem. B 2018, 122, 3572−3586